BIOCHEMISTRY
including biophysical chemistry & molecular biology

Article

pubs.acs.org/biochemistry

NMR Studies of the Dynamics of High-Spin Nitrophorins: Comparative Studies of NP4 and NP2 at Close to Physiological pH

Robert E. Berry,*[,†] Dhanasekaran Muthu,*[,‡] Fei Yang, and F. Ann Walker*

Department of Chemistry and Biochemistry, The University of Arizona, 1306 East University Boulevard, Tucson, Arizona 85721-0041, United States

Supporting Information

ABSTRACT: The β-barrel nitrophorin (NP) heme proteins are found in the saliva of the blood-sucking insect *Rhodnius prolixus*, which synthesizes and stores nitric oxide (NO) in the salivary glands. NO is bound to iron of the NPs and is released by dilution and an increase in pH when the insect spits its saliva into the tissues of a victim, to aid in obtaining a blood meal. In the adult insect, there are four nitrophorins, NP1−NP4, which have sequence similarities in two pairs, NP1 and NP4 (90% identical) and NP2 and NP3 (80% identical). The available crystal structures of NP4 have been used to propose that pH-dependent changes in the conformation of two loops between adjacent β-strands at the front opening of the protein, the A−B and G−H loops, determine the rate of NO release. At pH 7.3, NP4 releases NO 17 times faster than NP2 does. In this work, the aqua complexes of NP4 and NP2 have been investigated by nuclear magnetic resonance (NMR) relaxation measurements to probe the pico- to nanosecond and micro- to millisecond time scale motions at two pH values, 6.5 and 7.3. It is found that NP4-OH_2 is fairly rigid and only residues in the loop regions show dynamics at pH 6.5; at pH 7.3, much more dynamics of the loops and most of the β-strands are observed while the α-helices remain fairly rigid. In comparison, NP2-OH_2 shows much less dynamics, albeit somewhat more than that of the previously reported NP2-NO complex [Muthu, D., Berry, R. E., Zhang, H., and Walker, F. A. (2013) *Biochemistry 52*, 7910−7925]. The reasons for this major difference between NP4 and NP2 are discussed.

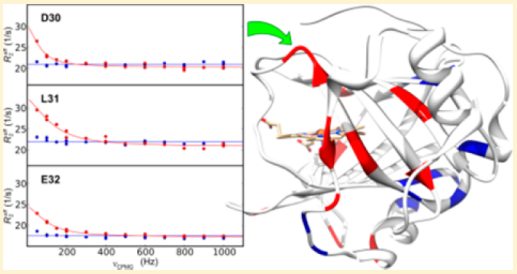

Nitrophorins (NPs) are ferriheme proteins that bind and carry nitric oxide and are found in the salivary glands of blood-sucking insects.[1−4] In the adult insect *Rhodnius prolixus*, which is native to the Amazon River basin, there are four such ferriheme proteins of the lipocalin fold (an eight-stranded β-barrel, with the heme protruding from the mouth of the barrel). The structures of various ligand complexes of NP1,[5−7] NP2,[8,9] and NP4[10−15] have been determined by X-ray crystallography. In the salivary glands, the hemes of the four proteins are bound to nitric oxide, which is synthesized by a constitutive nitric oxide synthase (NOS) enzyme found in the epithelial cells of the salivary glands.[16] When the insect finds a host that can provide the blood meal it needs each month, the cherry red saliva, including its nitrophorin proteins loaded with NO, is spit into the tissues of the host at the site of the bite.[4] Dilution of the proteins and the increase in pH from that of the saliva (5.0−6.0) to that of the host tissues (7.3−7.4) allow dissociation of NO, which can travel through cell walls to reach nearby blood capillaries. There it can interact with the heme enzyme guanylyl cyclase to produce cyclic GMP,[17] which causes vasodilation to allow more blood to be transported to the site of the wound, thus providing the insect with a blood meal in a relatively short time period. The four nitrophorins of the adult *Rhodnius* insect each have a molecular mass of ∼20 kDa, and they each have four conserved cysteine residues that form two disulfide bonds that help to maintain the eight-stranded β-barrel structures of each protein.[5−15]

Figure 1 shows the backbone structure of NP4, for which the largest number of crystal structures of the nitrophorins has been reported.[8,10−15] The protein sequences of the four proteins (shown in Figure S1 of the Supporting Information) fall into two pairs, NP1 and NP4, which are 90% identical in sequence, and NP2 and NP3, which are 80% identical. The abundances of NP1−NP4 in the insect saliva are 49, 21, 20, and 10%, respectively.[4] The two pairs of NPs have very different NO release rates, with NP4 and NP1 releasing NO 17 and 12 times faster than NP2, respectively, at pH 7.5 [k_{off} values of 1.6 and 1.1 s^{-1}, respectively (DOI: 10.1021/bi5013047), vs 0.093 s^{-1},[18] all at 27 °C and pH 7.5]. Understanding the dynamics of loop motions is very important for developing a full understanding of the behavior of the *Rhodnius* nitrophorins.

Montfort and co-workers have investigated the kinetics of release of NO from NP4 by stopped-flow kinetics,[19] by cryocrystallography and infrared spectroscopy of binding of NO and CO to NP4,[20] by femtosecond coherence spectroscopy (FCS) in combination with polarized resonance Raman spectroscopy and density functional theory (DFT) studies of binding of NO to NP4,[21] by ultrafast kinetics of release of NO from NP4,[22] and by two-dimensional Fourier transform

Received: October 17, 2014
Revised: December 5, 2014
Published: December 8, 2014

DOI: 10.1021/bi501305a
Biochemistry 2015, 54, 221−239

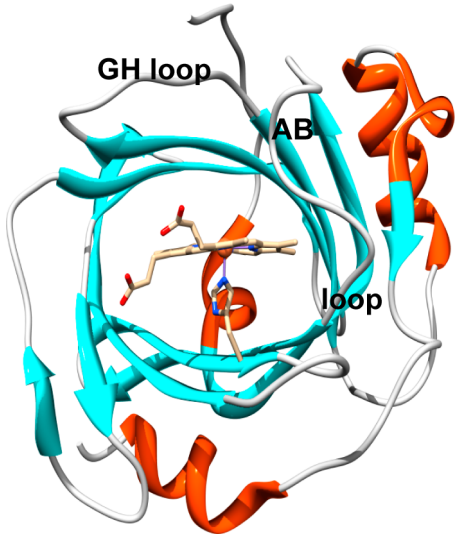

Figure 1. Ribbon drawing of the NP4-NO structure. The loops that move upon NO binding (A−B loop, residues 31−40, and G−H loop, residues 126−132) are labeled, and the heme is colored gold (stick representation); β-sheets are colored aqua, α-helices orange, and all loops gray.

infrared spectroscopy[23] to try to understand the mechanism of NO release. Knipp et al. have investigated the infrared and resonance Raman spectra of the Fe^{II}−CO complex and have studied association of CO to and dissociation of CO from Fe(II) NP4 and NP7 by nanosecond laser flash photolysis and stopped-flow kinetics.[24] In both cases of infrared investigations,[23,24] two vibrational frequencies were detected, one ascribed to the "closed loop" and the other to the "open loop" structure. Montfort et al. have found that the rate of dissociation of NO from NP4 is proportional to the open loop-state population, as well as to the pH-dependent kinetic amplitude of escape from the open pocket.[22] When both factors are considered, the off rate increases by more than 1 order of magnitude when the pH is changed from 5 to 8.[22] The fast phase of NO rebinding is assigned to a conformation of the ferric protein with a closed loop hydrophobic pocket, while the slow phase is assigned to the protein in an open loop conformation with a more hydrophilic heme pocket environment.[22,23]

In comparison to that of NP4, the rate of release of NO from native N-terminal NP2 changes by a factor of only 3 between pH 5 and 7.5,[18] suggesting that although all four nitrophorins have D29(30), not all are similarly affected by a change in pH, and that there is thus a need to investigate all four proteins by the same techniques, to determine the factors that affect the rates of NO release of each. In addition, NP2 shows no tendency to aggregate or form a dimer as a function of concentration and/or pH, whereas NP4 does at low pH (DOI: 10.1021/bi5013047). It is striking that the major difference between the A−B and G−H loops of NP2 and NP4 is that NP2 has one fewer amino acid in the A−B loop (Figure S1 of the Supporting Information), and that this could cause such dramatic differences between the behavior of NP2 and NP4 (if this is the factor that determines NO dissociation rates). A further difference is that NP4 and NP1 both have two prolines in the A−B loop, while NP2 and NP3 each have only one (Figure S1 of the Supporting Information). All four NPs have an aspartic acid as the last residue of β-strand A, and for NP4, Asp30 is believed to be the major factor that determines whether the A−B loop is open or closed.[19] Most crystal structures of NP4 determined at pH 5.6 show a hydrogen bond between the Asp30 side-chain carboxyl and Leu130 carbonyl.[11,12] Although all crystal structures of NP4-NO have the closed loop structure at all pH values, at pH 7.5 for other ligand complexes of NP4 this hydrogen bond is not present, the Asp30 oxygen and Leu130 carbonyl are much farther apart, and the A−B and G−H loops are "open".[10] No NP2 crystal structure determined at pH 6.5 shows a hydrogen bond between these two residues, Asp29 and Leu129,[8,9] and no lower-pH structures are available. The typical distance between the Asp29 carboxyl and Leu129 carbonyl in the pH 6.5 structures is 4.96 Å.[8,9]

We recently reported the dynamics of native N-terminal NP2-NO on the pico- to nanosecond and micro- to millisecond time scales at three pH values, 5.0, 6.5, and 7.3.[25] In that work, we used the Modelfree approach developed by Lipari and Szabo[26,27] and modified somewhat by others[28−32] for the pico- to nanosecond motion analysis and the Carr−Purcell−Meiboom−Gill (CPMG) experiment to investigate micro- to millisecond time scale dynamics.[33−40] It was found that at pH 5.0 and 6.5, NP2-NO is rigid and only a few residues in the loop regions show dynamics, while at pH 7.3, somewhat greater dynamics, particularly of the A−B loop (the loop connecting β-strands A and B), are observed.[25] Comparison to other lipocalins[41−50] showed that all are relatively rigid and that the dynamics of lipocalins in general are much more subtle than those of mainly α-helical proteins. Preliminary experiments during our study of NP2-NO showed that NP4, not bound to NO and thus containing high-spin Fe(III) ($S = {}^5/_2$), had much greater dynamics at pH 7.3 than did NP2 in the same high-spin Fe(III), $S = {}^5/_2$ state. Thus, when the dynamics study of NP2-NO had been completed, we began a detailed study of the dynamics of high-spin NP4. However, in that study, we were very limited in the pH range that we could use, because high-spin NP4 forms a homodimer at pH 5.0, which is not fully dissociated until at least pH 6.0, and we felt that to be sure we were not measuring the dynamics of dimer formation and/or dissociation, we could study NP4 at only pH ≥6.5. Detailed discussion of that homodimer and its properties is presented elsewhere (DOI: 10.1021/bi5013047). Interestingly, the NO complex of NP4 forms a much more stable homodimer than the NO-off protein does, and thus, the NO complex cannot be studied by NMR spectroscopy because ensuring that the protein is monomeric would require dilution to concentrations too low for NMR studies at pH 7.3−7.5 (DOI: 10.1021/bi5013047). The side chains shown to be important in dimer formation are D30, others in the A−B loop, and D132, as well as the heme carboxylates (DOI: 10.1021/bi5013047).

Unlike NP2, which favors one orientation of protohemin (which has no rotation axis passing through the heme plane), apo-NP4 and apo-NP1 bind both heme orientations equally well (see Scheme I of the Supporting Information). Therefore, to not have two equally intense $^1H\{^{15}N\}$ HSQC cross-peaks for many backbone amides that are near the heme, it is necessary to reconstitute the NP4 apoprotein with the so-called "symmetrical hemin", 2,4-dimethyldeuterohemin, in which the 2- and 4-vinyl groups of protohemin have been replaced with methyls. This produces a heme with two fewer carbons than protoheme, which could potentially change the dynamics of the protein by removing some steric interactions that may be

DOI: 10.1021/bi501305a
Biochemistry 2015, 54, 221−239

responsible for ruffling of the heme.[51] We will consider this possibility again in the Discussion.

Some readers may worry that the high-spin Fe(III) state ($S = {}^5/_2$) of NP2 and NP4 used in this study will cause peaks to be shifted far from where the diamagnetic peaks would be expected and/or to be severely broadened by the unpaired electrons. However, there have been a number of studies of the NMR spectra of paramagnetic proteins,[52−55] and these fears have been vastly exaggerated in many cases. As far as large shifts are concerned, the pseudocontact shifts of protein resonances are in most cases quite small, apart from those of the histidine ligand, where the peptide NH has −8 and −6.58 ppm pseudocontact shifts of the two nuclei[55] and contact shifts of 1.0 and 3.11 ppm. There are no contact shifts for protein resonances apart from those of His57(59), where despite the shifts and broadening, the His57 ^{15}NH group of high-spin NP2 was assigned in a sample of native N-terminal NP2 having [^{13}C,^{15}N]His present in the protein (116 and 2.90 ppm, respectively).[55] Peptide NH groups of high-spin NP4 residues very near His59 in β-strand C have not been assigned [Y58, Y60, and D61 (Figure S1 of the Supporting Information)], but the pseudocontact shift falls off as r^{-6}, where r is the distance of the ^{15}N from Fe (see Effect of Paramagnetism on R_1 and R_2 on page 2 of the Supporting Information); therefore, the ^{1}H{^{15}N} HSQC cross-peak for L57 was assigned (this work) but overlaps with another cross-peak. If it did not, we still would not use it in the dynamics analysis, because it is only 9.5 Å from Fe (see below).

Because the NO-off NP4 and native N-terminal NP2 aqua complexes are paramagnetic, relaxation of protons less than ∼13 Å from heme iron is expected to be significant.[52−55] In comparison, the effect on ^{15}N relaxation is reduced ∼100-fold because of the effect of the lower magnetogyric ratio of ^{15}N with respect to ^{1}H [$(\gamma_N/\gamma_H)^2 \sim 1/100$].[53] In fact, it has been shown that the effect of paramagnetic relaxation on ^{15}N nuclei located more than 7 Å from the heme iron in ferricytochrome b_5 ($S = {}^1/_2$) is negligible,[53] but the paramagnetic effect extends farther for $S = {}^5/_2$ native N-terminal NP2-OH$_2$ and NP4(sym)-OH$_2$. The effect of distance has been quantified: from comparison of R_1 and R_2 data for diamagnetic native N-terminal NP2-NO and $S = {}^5/_2$ native N-terminal NP2-OH$_2$, we find that amide ^{15}N nuclei more than 10 Å from Fe have a negligible effect on R_1 relaxation because of HS Fe^{III}. However, the effect on R_2 due to HS Fe^{III} extends much farther because the equations are different for the two; in fact, at 600 MHz for ^{1}H the effect on R_2 is roughly 25 times greater than that on R_1 (see Effect of Paramagnetism on R_1 and R_2 on page 2 of the Supporting Information). This eliminates all ^{15}N atoms that are within 13 Å of Fe, including ^{15}N atoms of V25−E32, D35−A45, A56−D61, D66−S72, A83−K88, Y104−T108, I119−G126, and L130−V136 of NP4, many of which we would very much like to probe. For the closer of these residues, their broad proton resonances usually make the peaks broad enough that they are not easily spotted and assigned, so the protein helps us not to include peaks from residues that should not be included. However, many of the residues listed above with ^{15}N closer than 13 Å were assigned. There are 93 residues whose backbone ^{15}N atoms are more than 13 Å from Fe, and we have used them. However, we find that inclusion or exclusion of the ^{15}N atoms that are between 10 and 13 Å from Fe does not change the parameters calculated from the Modelfree approach or the CPMG experiment. Thus, we have flagged those within that distance "orange peel" and provide both sets of information throughout the Results.

MATERIALS AND METHODS

Expression and Purification of Protein. Except where indicated, materials were obtained from Sigma-Aldrich and used without further purification; 2,4-dimethyldeuterohemin was obtained from Frontier Scientific (Logan, UT). Native N-terminal NP2,[18] labeled with ^{15}N, was prepared as reported previously.[25]

NP4 is the only *Rhodnius* nitrophorin that, when expressed recombinantly, has its native first residue (alanine) and has no Met(0) preceding it, as is the case for NP1−NP3. NP4 is usually expressed under conditions that produce inclusion bodies.[56] When these inclusion bodies are renatured and purified, followed by the addition of hemin, a stable holoprotein is produced. Thus, ^{15}N-labeled NP4 was readily prepared as reported previously,[25,56] including size-exclusion FPLC on a GE Healthcare HiPrep 26/60 Sephacryl 5−100 size-exclusion column with one or two 5 mL guard columns preceding it.[25,57]

Triple-resonance experiments required for the assignment of the protein backbone need large amounts of ^{13}C and ^{15}N isotopically enriched protein. Thus, the same high-yielding inclusion body method that was employed for the NP2(D1A) construct[58] in our NP2-NO study[25] to prepare doubly labeled NP4 was used here. The natively folded, soluble apoprotein was concentrated to ∼50 mL and titrated with 2,4-dimethyldeuterohemin (5 mL of ∼2 mM 2,4-dimethyldeuterohemin dissolved in a few drops of 1 M KOH and diluted into pH 7.5, 100 mM sodium phosphate buffer) to form the holoprotein. The pH was reduced to 5.5 with acetic acid, and the excess 2,4-dimethyldeuterohemin precipitate was then removed by high-speed centrifugation and saved for potential use with later samples of apo-NP4. The sample was further concentrated to ∼5 mL before being loaded onto a gel filtration column [a 5 mL prepacked HiTrap desalting guard column connected in series with a GE Healthcare HiPrep 26/60 Sephacryl S-100 HR size-exclusion column, equilibrated with 100 mM sodium acetate buffer (pH 5) and 100 mM NaCl]. The peak fraction that eluted from the size-exclusion column as the dimer of NP4 was dialyzed against 30 mM sodium acetate buffer (pH 5) before being further purified by cation exchange chromatography. In ≤5 mg batches, the dialyzed nitrophorin was loaded onto a cation exchange column (two 5 mL HiTrap SP HP columns connected in series), washed with 20 mL of the 30 mM sodium acetate buffer (pH 5), and eluted with a salt gradient (1 M NaCl in 30 mM sodium acetate buffer). Pure [U-^{13}C,^{15}N]NP4 reconstituted with the symmetrical hemin eluted as a single peak at an ionic strength of ∼4 mS/cm. The final yield of [U-^{13}C,^{15}N]NP4 was ∼10 mg/L of minimal growth medium.

Preparation of NMR Samples. Stocks of NMR buffers were prepared at pH 6.5 (50 mM sodium acetate with 95% H_2O and 5% D_2O) and pH 6.5 and 7.3 (both 50 mM sodium phosphate with 95% H_2O and 5% D_2O). The purified [U-^{15}N]NP2, [U-^{15}N]NP4, and [U-^{13}C,^{15}N]NP4 proteins were exchanged four times into the appropriate NMR buffer (using Centriprep 10000 MWCO centrifuge concentrators) and loaded into Shigemi NMR tubes. Sodium 3-(trimethylsilyl)-1-propanesulfonate (DSS) (from Cambridge Isotope Laboratories, Inc.) was added to the samples as a chemical shift reference. The concentrations of the [U-^{15}N]NP2, [U-^{15}N]NP4, and [U-^{13}C,^{15}N]NP4 samples were ∼1.0, ∼1.0,

DOI: 10.1021/bi501305a
Biochemistry 2015, 54, 221−239

and ~3.7 mM, respectively, at pH 7.3 and for [U-^{15}N]NP4 at pH 6.5, two samples, 0.2 and 0.8 mM.

Sequence-Specific Assignments of [^{13}C,^{15}N]NP4 and Relaxation Data for [^{15}N]NP2 and [^{15}N]NP4. Two-dimensional (2D) ^{1}H{^{15}N} HSQC spectra were initially used to identify the number of spin systems. The assigned HSQC spectrum of doubly labeled NP2(D1A)-NO at pH 7.3 could be used to identify some of the peaks of a high-spin ^{15}N-labeled native N-terminal NP2 sample, but further assignments using a doubly labeled sample were not attempted, because the amount of dynamics observed for native N-terminal NP2, though slightly greater than for NP2-NO,[25] was so much smaller than that observed for NP4 that it was decided that little new information could be gained about NP2 dynamics except that the high-spin NP2 was much more rigid than NP4. Thus, the dynamics data for high-spin NP2 are reported in terms of peak numbers rather than assigned protein amino acids.

The 2D and three-dimensional (3D) heteronuclear NMR spectra for the sequence-specific assignments of [U-^{13}C,^{15}N]NP4 at pH 7.3 were recorded at the National Magnetic Resonance Facility at Madison (NMRFAM) on a 600 MHz Bruker AVIII-600i instrument equipped with a 5 mm TXI cryoprobe. Relaxation data for [U-^{15}N]NP4 and [U-^{15}N]NP2 were collected on a 600 MHz Varian NMR spectrometer equipped with a cryogenic probe, at both pH 7.3 and 6.5. In all cases, the temperature was maintained at 30 °C. 2D ^{1}H{^{15}N} HSQC, 3D HNCA, 3D HN(CA)CO, 3D HNCO, 3D HNCACB, and 3D CBCA(CO)NH peak lists for NP4 were used as input to the PINE server[59] and, employing the PINE-SPARKY extension,[60] were used to determine sequence-specific backbone resonance assignments. Assignment data were collected at pH 7.3 for NP4, referenced to DSS,[61] and are listed in Table S1 of the Supporting Information. This is a summary of all the backbone chemical shifts assigned and represents an average of all of the assignments of the experiments listed in Appendix A of the Supporting Information. The amide ^{15}N shifts were obtained from the assignments of the ^{1}H{^{15}N} HSQC experiment (Table A1 of the Supporting Information). The Cα chemical shifts were obtained from the assignments in the HNCA experiment (Table A2 of the Supporting Information). The carbonyl chemical shifts were obtained from the assignments in the HNCO experiment and the HN(CA)CO experiment (Table A3 of the Supporting Information). The Cα and Cβ chemical shifts are the averages obtained from the assignments of the HNCACB and CBCA(CO)NH experiments (Table A4 of the Supporting Information). The amide ^{1}H shifts are the averages obtained from the assignments of the ^{1}H{^{15}N} HSQC, HNCA, HN(CA)CO, HNCO, HNCACB, and CBCACONH experiments (Tables A1−A4 of the Supporting Information). These chemical shifts were used to obtain backbone torsional angles using *TALOS* (Torsion Angle Likelihood Obtained from Shift and sequence similarity),[62−64] specifically the version *TALOS-N*[64] (which also derives side-chain χ_1 angle information), and report an estimated backbone order parameter S^2 derived from the chemical shifts.[65] The pH 7.3 assignments obtained for NP4 could be transferred to pH 6.5 by preparing a series of variable-pH samples having intermediate pH values between the two pH values, and following the movements of the relatively few peaks that moved. However, this was true only for the ^{1}H{^{15}N} HSQC assignments; side-chain assignments could not be transferred to pH 6.5. All data were processed with the *NMRPipe*[66,67] suite and visualized with *SPARKY*.[68] All relaxation data for [U-^{15}N]NP4 are listed in Tables S3−S5 of the Supporting Information; Modelfree dynamic parameters are listed in Tables S6−S9 of the Supporting Information, and all CPMG data are listed in Tables S10−S12 of the Supporting Information. As a function of peak number rather than assignment, relaxation data for [U-^{15}N]NP2 at pH 7.3 are listed in Table S13 of the Supporting Information and CPMG data for NP2 are listed in Table S14 of the Supporting Information.

^{15}N Relaxation and Modelfree Calculations. ^{15}N longitudinal (T_1) and transverse (T_2) relaxation and ^{15}N{^{1}H} NOE experiments were performed at 30 °C for one sample of native N-terminal [U-^{15}N]NP2 (1.0 mM, pH 7.3), one sample of [U-^{15}N]NP4 reconstituted with the symmetrical hemin (1.0 mM, pH 7.3), and two samples of [U-^{15}N]NP4 reconstituted with the symmetrical hemin (0.8 and 0.2 mM) at pH 6.5 on a Varian 600 MHz spectrometer in an interleaved manner with a few duplicate points for error estimation. T_1 and T_2 data were collected with 64 scans for the 0.8 mM sample and 128 scans for the 0.2 mM sample, with 1024 × 200 complex data points in each case. A recycle delay of 1.5 s was used between the scans. For T_1 measurements, a total of 13 spectra were recorded using T_1 delays of 0.01, 0.02 (two times), 0.06, 0.12 (two times), 0.22, 0.42 (two times), 0.64, 0.96 (two times), and 1.28 s. For T_2 measurements, a total of 14 spectra were recorded using T_2 delays of 0.01, 0.03 (two times), 0.05, 0.07 (two times), 0.09, 0.11 (two times), 0.13, 0.15 (two times), 0.17, and 0.19 s (duplicates are indicated). The ^{15}N{^{1}H} NOE data were acquired with 256 scans in a 1024 × 120 data matrix with a recycle delay of 4.5 s in an interleaved fashion. The T_1, T_2, and ^{15}N{^{1}H} NOE relaxation data were analyzed using *SPARKY*.[68] The intensities of the amide resonances were obtained by measuring the heights of the peaks in the spectra, a routine available within *SPARKY*. Uncertainty measurements were made from duplicate spectra acquired independently.

Relaxation rates R_1 and R_2 were obtained by exponential curve fitting of relaxation times T_1 and T_2 using *RELAX*.[69] *RELAX* was also used to calculate the ^{15}N{^{1}H} heteronuclear steady-state NOEs from the I_{sat}/I_{unsat} ratios, where I_{sat} and I_{unsat} are the peak intensities in the spectra collected with and without proton saturation, respectively. Uncertainty measurements for model-free calculations were obtained using *RELAX*, either from duplicate spectra acquired independently or from spectral noise using the baseplane error estimation routine available within the program. The estimated errors are in the range of 2−4% for R_1 and R_2 and 4−8% for the NOE, with few exceptions. An initial guess of the molecular rotational diffusion tensor and overall correlation time (τ_m) was obtained from the R_2/R_1 ratio of the individual ^{15}N amide peaks using the programs r2r1_tm and quadric_diffusion developed by the Palmer group,[3T] which follows the approach of Brüschweiler et al.[70] and Lee et al.[71] The X-ray structure of NP4 [Protein Data Bank (PDB) entry 3C78, the structure of NP4 bound to the symmetrical hemin and to NH_3 at pH 7.5] was used for this purpose and for subsequent Modelfree calculations. The PDB file for Modelfree calculation was prepared by adding hydrogen atoms using UCSF-Chimera[72] followed by translation to the center of mass with the program "pdbinertia" developed by the Palmer group. The final PDB file was used as input for the model-free calculations.

The FAST-Modelfree program developed by Cole and Loria[32] was used to accomplish the model-free calculations. The FAST-Modelfree program interfaces with Modelfree

DOI: 10.1021/bi501305a
Biochemistry 2015, 54, 221−239

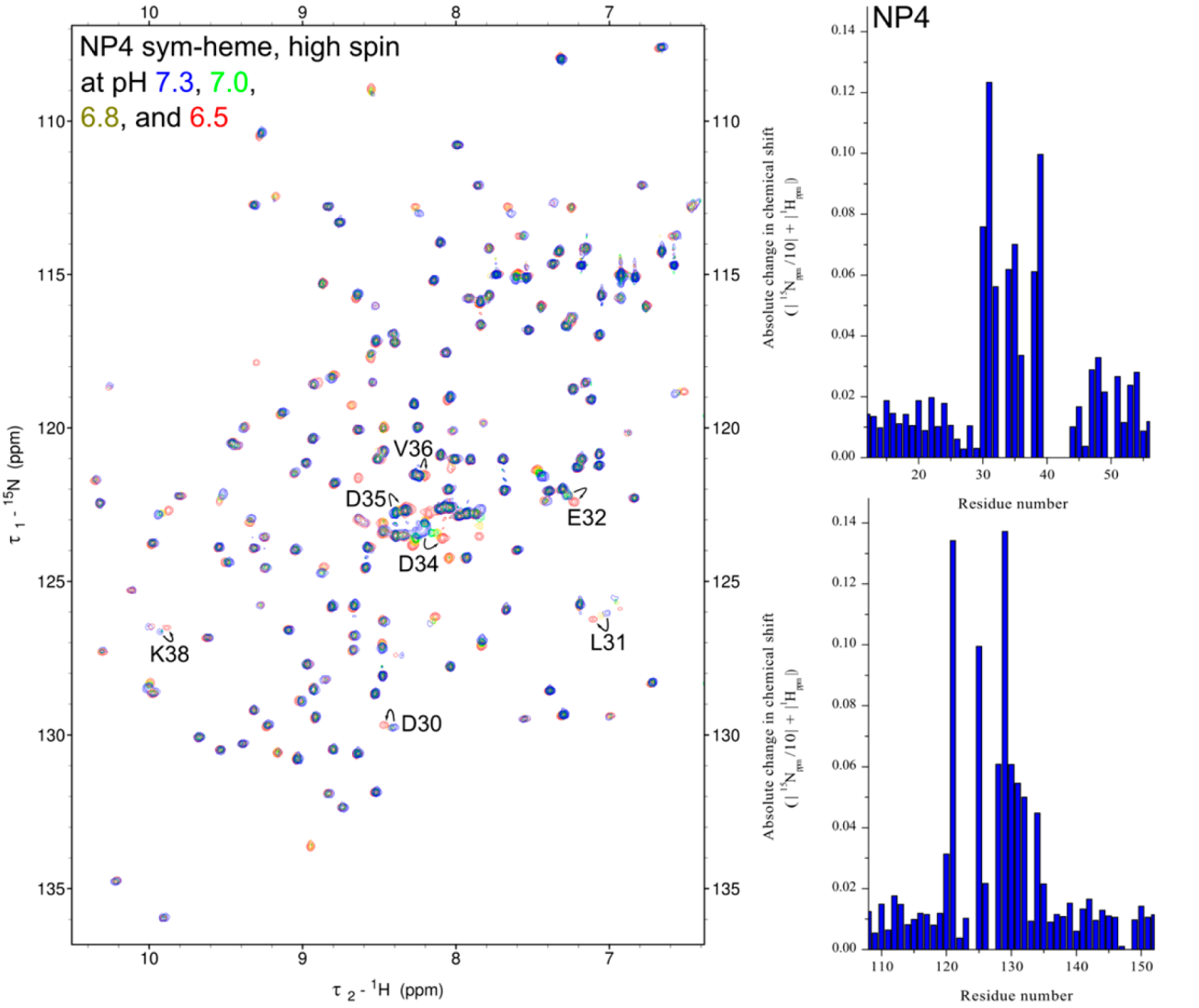

Figure 2. $^{1}H\{^{15}N\}$ HSQCs (left) of high-spin NP4 at pH 7.3 (blue) and 6.5 (red), and two intermediate pH values (green and tan), showing how the peak assignments could be followed between the two pH values. A full-page version of the pH 7.3 data, with complete assignments, is shown in Figure S2 of the Supporting Information, and additional details of the assignments are shown in Figure S1 of the Supporting Information. Magnified plots (right) of the absolute change in chemical shift for ^{15}N and ^{1}H (with the latter emphasized by a factor of 10), for residues 12−56 (top, A−B loop, residues 30−40) and 108−152 (bottom, G−H loop, residues 125−131). These magnified plots are shown in larger form in Figure S3 of the Supporting Information.

version 4.1 developed by the Palmer group to perform the rigorous statistical testing protocols for the assignment of model functions for each individual residue. Moreover, it requires minimal user involvement in preparing the input files. The ^{15}N chemical shift anisotropy (CSA) and the N−H bond length (r_{N-H}) used in the calculations were −172 ppm and 1.02 Å, respectively, which seem to be good choices as they have been used in most of the recent protein dynamics studies.[74] The FAST-Modelfree configuration file, showing all the parameters used in the calculations, is provided as Table S15 of the Supporting Information. The results from "quadric diffusion" calculations, especially the $D_{\parallel}/D_{\perp}$ ratio, suggested an axially symmetric diffusion tensor for the model-free calculations. Thus, of two available choices (isotropic or axially symmetric) for the diffusion tensor in the FAST-Modelfree program, an axially symmetric diffusion tensor was chosen for all calculations.

Relaxation Dispersion Analysis of NP4 Data at pH 7.3 and 6.5 and NP2 Data at pH 7.3. All of the ^{15}N R_2 relaxation experiments were conducted on a Varian 600 MHz spectrometer at 30 °C using the relaxation-compensated CPMG pulse sequence described previously by Kay et al.[33] One sample of native N-terminal [U-^{15}N]NP2 (1.0 mM, 30 °C) and one sample of [U-^{15}N]NP4 reconstituted with the symmetrical hemin (1.0 mM, 30 °C) were studied at pH 7.3, and two samples, 0.8 and 0.2 mM, of [U-^{15}N]NP4 reconstituted with the symmetrical hemin were studied at pH 6.5 and 30 °C. The constant time delay was set to 0.08 s in all cases. A series of 22 spectra were recorded with CPMG, with ν_{cp} values of 66.7, 133.3, 200 (two times), 266.7, 333.3, 400 (two times), 466.7, 533.3, 600 (two times), 666.7, 733.3, 800 (two times), 866.7, 933.3, and 1000 Hz (two times) (duplicates are indicated). In addition, a reference spectrum without any CMPG component in the pulse sequence was also recorded in duplicate. Each 2D spectrum was acquired as a complex 512 × 256 data matrix with 32 scans per free induction decay and a 2.2 s delay between scans. *SPARKY*[68] was used to analyze the data to obtain the peak heights for curve fitting to obtain the

DOI: 10.1021/bi501305a
Biochemistry 2015, 54, 221−239

effective transverse relaxation rates (R_2^{eff}). The program *NESSY*[73] was used for curve fitting. The *SPARKY* peak height list files were directly used in *NESSY*.

For high-spin native N-terminal NP2, because all ^{15}N relaxation data showed flat relaxation plots, R_2 versus delay (no observed decay curves), $\Delta R_2^{eff}(\nu_{CPMG})$ two-point values were calculated using the following equation:

$$\Delta R_2^{eff}(\nu_{CPMG}) = (1/T_{cp}) \ln I_{1000}/I_{50} \quad (1)$$

where I_{1000} and I_{50} are the heights of cross-peaks in spectra collected at effective CPMG fields of 1000 and 50 Hz, respectively, and T_{cp} is the constant time delay (0.06 s).

RESULTS

Backbone Sequential Assignment of NP4 and Analysis of the Chemical Shifts at pH 7.3. It is necessary to have the ^{15}NH assignments to fully interpret the relaxation data. We have this for NP4 but not NP2. The HNCACB and CBCACONH experiments were conducted on uniformly ^{13}C- and ^{15}N-enriched NP4 samples reconstituted with the symmetrical hemin to effect the sequential assignments. The $^1H\{^{15}N\}$ HSQC plot of [U-^{15}N]NP4 at pH 7.3 is shown as blue spots in Figure 2, and the peaks that move between pH 7.3 and 6.5 are shown in two shades of green at two intermediate pH values and, finally, in red at pH 6.5. To the right of the HSQC map is shown a magnified scale rendering of the absolute change in ^{15}N and ^1H chemical shifts between pH 6.5 and 7.3 for residues from the A−B (top) and G−H (bottom) loops. As one can see, even over this relatively small pH change, the residues of these loops show chemical shift changes much larger than those of other residues in the protein. These observations are consistent with the changes in the A−B and G−H loop conformations seen in X-ray crystallographic structures of NP4 obtained at pH 5.6 and 7.5.[8−15] A complete map of the assigned cross-peaks at pH 7.3, in full-page size with all assigned peaks labeled, is shown in Figure S2 of the Supporting Information, with more details of the assignments included in Figure S1 of the Supporting Information. The ^1H, ^{15}N, and ^{13}C of CO, CA, and CB chemical shifts of NP4 at pH 7.3 are presented in Table S1 of the Supporting Information. Complete assignment data for NP4 at pH 7.3 are presented in the four tables of Appendix 1 of the Supporting Information.

As seen clearly in Figure 2, the observed chemical shift values of backbone protons and nitrogens of ^{15}N-labeled NP4 are quite similar at pH 7.3 and 6.5 for all residues except those located in the A−B and G−H loops; in some cases, an up to 0.15 ppm change in ^{15}N chemical shifts occurs over this pH range, and in some cases, a >0.2 ppm change in proton chemical shift is seen. At pH 7.5, we investigated the *TALOS*[62] suite of programs using the chemical shifts of NP4. *TALOS-N*[64] is an improved version of the very commonly used *TALOS+* software,[63] for empirical prediction of protein backbone dihedral angles (ϕ and ψ) to within ±13° of the crystal structure values from experimentally determined chemical shift values. *TALOS-N* also derives side-chain χ_1 angle information and reports an estimated backbone order parameter S^2 derived from the chemical shifts.[65] A plot of *TALOS-N*-derived S^2 versus NP4 residue number is shown in Figure 3, and a summary of the output from *TALOS-N*[64] is listed in Table S2 of the Supporting Information.

In Figure 3, one can see that all of the loops of the structure are clearly identified, in terms of their increased level of disorder, by lower *TALOS-N*-derived S^2 values, and that the long loop after the disulfide bond between C2 and C122 shows significant disorder, as does the short loop between α_1 and β_A. The A−B loop shows disorder, with a marked increase in the level of order in the vicinity of Val36 and Pro37 (the latter of which is not probed in the $^1H\{^{15}N\}$ HSQC experiment). The β_B strand shows significant disorder, culminating with the very short B−C loop, residues 49−52, and although residues 57−61 of β_C (including His59, the protein-provided heme ligand) are too close to high-spin Fe(III) to be resolved, we see the disorder of the C−D loop residues that follow (residues 63−66). The long E−F loop, residues 91−102, shows significant disorder that is much more resolved than that of the G−H loop (residues 125−131). The β_H−α_2 loop, residues 139−146, also shows significant disorder, as does the α_2−α_3 loop, residues 157−175. Helix α_3 also shows significant disorder by the *TALOS-N* plot criteria.

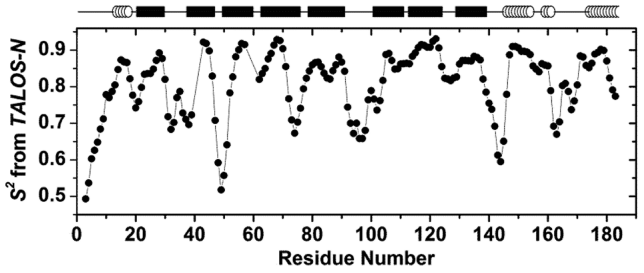

Figure 3. Plot of order parameter S^2 obtained from *TALOS-N*[64] vs NP4 residue number, showing the large change in order and/or disorder.

The predicted order parameters (S^2) calculated from *TALOS-N*[64] show reduced values associated with protein loop regions and increased dynamics at pH 7.3, most notably at the A−B and G−H loop regions near the opening to the heme pocket. The predicted ϕ and ψ angles are very similar at pH 7.3 to those of the crystal structure at pH 7.5 (PDB entry 3C78), with the exception of some of the residues in the A−B and G−H loops, suggesting that the structure of the loop regions is fairly similar to that of the crystal structure. NP4 structures obtained at low pH show a 3_{10} helix for the three residues P33, D34, and D35, but we cannot probe the *TALOS-N* predictions in solution at low pH because of the dimerization of NP4 at low pH (DOI: 10.1021/bi5013047).

Some of the predicted ϕ and ψ angles are not reliable because of dynamics and a lack of consensus in database matches. These are labeled "Dynam" or "Warn", and we have excluded these [in Table S2 of the Supporting Information, F18, D21, P33, K38, G51, P62, K63, T64, K81, F86, V99, N103, Y104, T106, K128, D129, L130, L133, L137, R139, T157, E168, N170, and C171 (24 in total)]. Of these, 13 are in loops and would thus be expected to deviate in some way from the crystal structure (underlined in the list above). As we will show below, the CPMG analysis also identifies many more residues that have dynamics that might affect predictions of ϕ and ψ angles; F86, N103, Y104, and T106 fit to model 3. That leaves only seven unexplained backbone deviations, of which three were assigned to model 1 (F18, D21, and K81), and four were not assigned to a model (L133, L137, E168, and N170). These observations, combined with increased R_2 values (described in the next section) and k_{ex} values (described in the CPMG section), suggest that dynamics, and not structural changes, could be the reason for the chemical shift differences

DOI: 10.1021/bi501305a
Biochemistry 2015, 54, 221−239

observed at pH 7.3. *TALOS-N*[64] analysis also revealed that the conformations of the A−B and G−H loops are very similar in solution to those seen in the crystal structure of NP4-NH_3 at pH 7.5 (PDB entry 3C78), as is true for other parts of the protein (Table S2 of the Supporting Information). At pH 7.3, the loops should be open, as they are at pH 7.5 (PDB entry 3C78). Thus, one would not expect major conformational differences as a function of ligand.

In Figure S4 of the Supporting Information is shown a comparison of amide N−Fe distances in angstroms and the HSQC cross-peak signal-to-noise ratio (S/N), both as a function of NP4 residue number. (Amide N−Fe distances are given numerically in Table S9 of the Supporting Information.) As shown in Figure S4 of the Supporting Information, the N−Fe distances correlate well with the S/N profile, which supports the expectation that the $(\gamma_N/\gamma_H)^2 \sim 1/100$ effect on resonance broadening[53] would make $^1H\{^{15}N\}$ HSQC cross-peaks observable (R_1 criterion) if the ^{15}N is >10 Å from Fe.

Fast Time Scale Dynamics. It is well documented in the literature that the fast time scale motions (picoseconds to nanoseconds) of proteins can be derived from a suite of relaxation experiments: ^{15}N longitudinal relaxation rate (R_1), transverse relaxation rate (R_2), and steady-state $^{15}N\{^1H\}$ NOE.[26,27,74,75] For high-spin NP4(sym), these measurements were taken at two different pH values, 7.3 and 6.5. As mentioned in the introductory section, we have shown in separate work that NP4 dimerizes at low pH and is essentially fully dimeric at pH 5.0. The following paper in this issue describes this dimerization (DOI: 10.1021/bi5013047). On the basis of the work reported therein (DOI: 10.1021/bi5013047), although we are quite sure that at pH 7.3, a 1 mM solution of NP4(sym) in the absence of NO or other exogenous ligands is at least 99.9% monomeric, we were not entirely certain that the same would be true at pH 6.5. Thus, for this study of the dynamics of NP4(sym), we investigated the dynamics at pH 6.5 at two concentrations, 0.8 and 0.2 mM. We find that the R_1 values increase on average by ∼16.8% on dilution, while the R_2 values decrease by ∼8.6% on dilution. This is as expected, because of the difference in the viscosity of the two samples, the more dilute one having the lower viscosity. The steady-state NOE values vary in magnitude and sign as the sample is diluted, from an average of 3.57% for 82 residues to −3.74% for 50 residues. However, despite all of our checks of the experimental data, Modelfree calculations showed that the 0.2 mM sample data were much more difficult to fit, could not assign a model to 35 residues that were assigned for the 0.8 mM sample, and produced unreliable values of R_{ex} and τ_e for the residues it was able to fit. This made it unclear whether there was a monomer/dimer contribution to the 0.8 mM concentration data at pH 6.5. The numbers of transients for the R_1, R_2, and NOE experiments were increased by a factor of 2 for the 0.2 mM sample as compared to that for the 0.8 mM sample, thus requiring 48 h for the R_2 experiment rather than 24 h, for example; however, it was impractical to increase the number of transients beyond that, in particular by a factor of 16, the square of the change in concentration, and more transients would also have increased the likelihood of introducing more noise spikes or other artifacts. Thus, although we have included all data and their fits to the Modelfree calculations, we are left with the nagging question of whether any of the pH 6.5 data are as reliable as we would like.

The $^1H\{^{15}N\}$ HSQC spectra of both pH 7.3 and 6.5 samples of NP4(sym) are very well dispersed, as shown in Figure 2 (blue and red cross-peaks, respectively). Sequential assignments of the corresponding doubly labeled NP4(sym) sample at pH 7.3 were made without any difficulty for all the residues except Ala1, Cys2, Asn5, Gly11, Val25, (Pro33), (Pro37), Tyr40, **Cys41**, **Ala42**, **Ala43**, Ser50, **Tyr58**, **His59**, **Tyr60**, **Asp61**, (Pro62), **Phe68**, **Asp70**, Leu79, Gly80, **Thr121**, **Cys122**, **His124**, Asn127, Lys148, Thr166, Ala172, and Tyr173. Many of these could not be assigned because they were within 10 Å of the heme iron with its five unpaired electrons (bolded and underlined in the list above); however, it was possible to assign several of the residues with backbone ^{15}N values of <10 Å [L57 (9.49 Å), Y105 (9.75 Å), L123 (7.75 Å), and Y134 (9.59 Å)]. Also, a total of 26 assigned peaks could not be included in the model-free analysis calculations for the corresponding ^{15}N-labeled NP4(sym) at pH 7.3 and 24 at pH 6.5 because their signal overlapped with that of another residue. This is in addition to the residues that are unassigned and three proline residues that lack an amide proton. Thus, a total of 55 of 184 residues were not included in the calculations at pH 7.3 and 54 of 184 residues at pH 6.5. Of those that were included, three were excluded at each pH on the basis of very large experimental errors or S^2 values that were 1.0.

All the residues in the two loops of interest except Pro33, Val36, Pro37, Arg39, and Tyr40 (A−B loop) and Asn127, Asp129, Gly131, and Asp132 (G−H loop) were assigned without any ambiguity and did not overlap with other $^{15}N-^1H$ cross-peaks and were thus included in the model-free analysis at pH 7.3. Some peaks were better resolved at pH 6.5 than at pH 7.3, and some peaks that overlapped at pH 7.3 did not overlap at pH 6.5. However, all of the ^{15}N atoms of the residues of the A−B and G−H loops are within 13 Å of high-spin Fe^{III} and, as we show in Effect of Paramagnetism on R_1 and R_2 on page 2 of the Supporting Information, should not be used for the Modelfree analysis. Although the R_1 data for ^{15}N more distant than 10 Å should be unaffected by paramagnetism, for R_2 the effect extends to 13 Å. We have, however, left the data for residues with their ^{15}N atoms within 10−13 Å of Fe in the tables, clearly marked, for these data do not differ from those for residues with their ^{15}N atoms more than 13 Å from Fe; the R_1, R_2, NOE, and S^2 averages are essentially unchanged by inclusion or exclusion of the 34 residues whose backbone ^{15}N atoms are within 10−13 Å of Fe.

The R_1, R_2, and NOE values measured for NP4(sym) at pH 7.3 and 1.0 mM (green), pH 6.5 and 0.8 mM (red), and pH 6.5 and 0.2 mM (black) are shown in Figure 4. The R_1, R_2, and NOE values for some of the residues show large deviations in range from the average values, and the pH 6.5, 0.2 mM sample data tend to show the most extreme values. Overall, the pH 7.3, 1.0 mM data show the smallest R_1 values and the largest R_2 values, while the pH 6.5, 0.2 mM sample had the largest R_1 values and the smallest R_2 values, because of viscosity effects, with the NOE data being mixed. All R_1 data at pH 7.3 and 6.5 are summarized in Table S3 of the Supporting Information; all R_2 data at both pH values and all concentrations are summarized in Table S4 of the Supporting Information, and all NOE data at both pH values and all concentrations are summarized in Table S5 of the Supporting Information. The deviations did not follow any pattern that would indicate correlated motions of loops. For the Modelfree analysis, as mentioned above, the X-ray structure of NP4 reconstituted with the symmetrical hemin and bound to ammonia (PDB entry 3C78) was chosen because it is the only structure of the symmetrical hemin complex and was refined to 0.98 Å

DOI: 10.1021/bi501305a
Biochemistry 2015, 54, 221−239

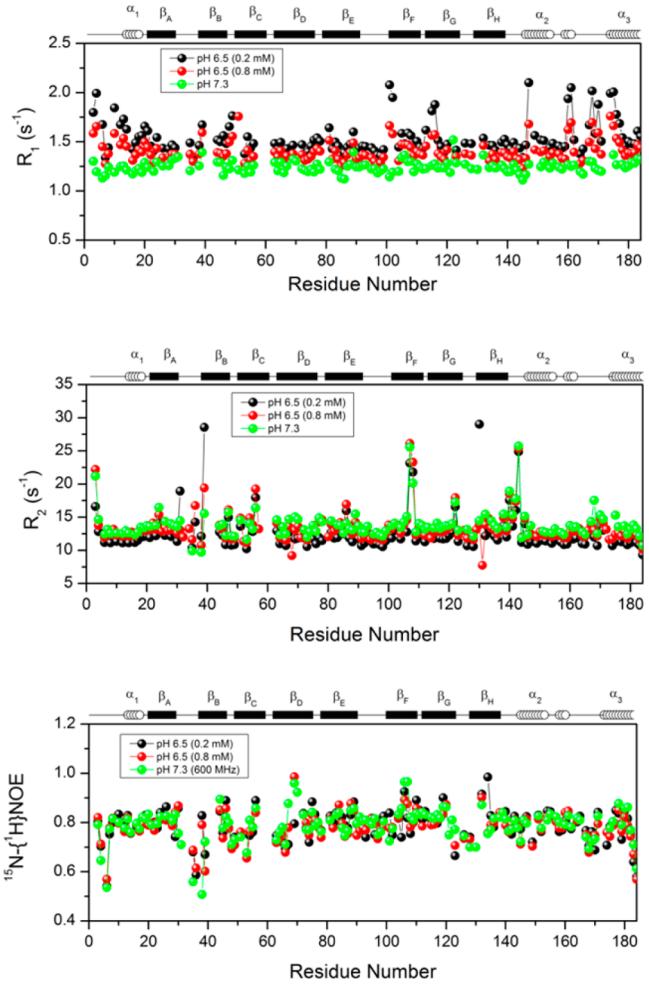

Figure 4. R_1, R_2, and NOE ^{15}N relaxation data for high-spin NP4 obtained at 600 MHz, measured at pH 7.3 and 1.0 mM (green), pH 6.5 and 0.8 mM (red), and pH 6.5 and 0.2 mM (black). The Modelfree order parameters were obtained by fitting the raw data to the Lipari−Szabo Modelfree formalism using FAST-Modelfree as described in Materials and Methods. Errors are not shown for the sake of clarity. The locations of β-sheets and α-helices are shown above the plot. At pH 7.3, a total of 58 non-proline residues could not be included in the calculation because of overlap (26 residues), not being found (16 residues), or not being assigned (16 residues); at pH 6.5 and 8 mM, a total of 56 non-proline residues could not be included in the calculation because of overlap (24 residues), not being found (16 residues), or not being assigned (16 residues).

resolution. It was interesting to note that the distances of each ^{15}N from Fe of the vast majority of residues of PDB entry 3C78 were slightly smaller (~0.15 ± 0.05 Å) than those of structures of the protohemin complex of NP4, for example, PDB entry 1X8P, also an NP4-NH_3 structure. Protohemin has two additional atoms, the 2- and 4-vinyl β-carbons, compared to the symmetrical hemin, 2,4-dimethyldeuterohemin.

The analysis of the dynamics of a protein uses the program *FAST-Modelfree* (J. P. Loria, Yale University, New Haven, CT),[31] which interfaces with *Modelfree* version 4.1 (A. G. Palmer, Columbia University, New York, NY) or the more recent program *RELAX* (version 3.0).[76−78] We have utilized *FAST-Modelfree* for most analyses of the contributions of microsecond to millisecond exchange phenomena to transverse relaxation (R_{ex}). The extended model-free spectral density function $J(\omega)$ can be fit to NMR spin relaxation data, assuming an axially symmetric diffusion tensor:

$$J(\omega) = 2/5 \sum_{j=1}^{3} A_j \left[\frac{S^2 \tau_j}{1 + (\omega\tau_j)^2} + \frac{(1 - S_f^{\,2})^2 \tau_f'}{1 + (\omega\tau_f')^2} + \frac{(S_f^{\,2} - S^2)\tau_s'}{1 + (\omega\tau_s')^2} \right] \quad (2)$$

where $\tau_1^{-1} = 6D_\perp$, $\tau_2^{-1} = D_\parallel + 5D_\perp$, $\tau_3^{-1} = 4D_\parallel + 2D_\perp$, $\tau_s' = \tau_j\tau_e/(\tau_j + \tau_e)$, where τ_e is either τ_f or τ_s, $A_1 = (3\cos^2\theta - 1)^2/4$, $A_2 = 3\sin^2\theta\cos^2\theta$, $A_3 = {}^3/_4 \sin^4\theta$, and θ is the angle between the N−H bond vector and the unique axis of the diffusion tensor. Five representations of the spectral density function were considered. The first model (M1) was based on the single-time scale model-free formalism given in eq 2, fitting S^2 alone ($\tau_f = \tau_s = 0$). The second model (M2) incorporated the presence of fast internal motions (τ_f < 100−200 ps) by fitting both S^2 and $\tau_e = \tau_f$. The third (M3) and fourth (M4) models added an $R_{ex,app}$ term to the model-free formalism to take into account the loss of transverse magnetization caused by conformational exchange and provided fits to S^2 and $R_{ex,app}$ (M3) and S^2, $\tau_e = \tau_f$, and $R_{ex,app}$ (M4), respectively. The last model (M5) considered the presence of internal motions slower than τ_f but faster than the overall rotational correlation time of the protein (τ_m) by fitting S_f^2, S^2, and $\tau_e = \tau_s$. The five dynamic models were fit to the experimental data for each resonance while holding the value of τ_m fixed at the value determined from the R_2/R_1 ratio. A grid search was used to obtain initial estimates for the values of the remaining model parameters as described elsewhere.[50] Statistical properties of the Modelfree parameters were obtained from Monte Carlo simulations,[79] implemented in FAST-Modelfree. Model selection was conducted according to the protocol outlined by Mandel et al.[31] and implemented in FAST-Modelfree.

The initial estimate of the overall correlation time (τ_m) and the ratio of parallel to perpendicular rotational diffusion motional tensor, D_{ratio} ($D_\parallel/D_\perp$), of NP4(sym) at pH 7.3 was calculated from the R_2/R_1 ratio using the program *quadric_diffusion* (A. G. Palmer, Columbia University). This gave a τ_m value of 9.4 ns as the overall correlation time and a value of 1.09 as the D_{ratio}, which was used in the model-free calculations. The relaxation data were analyzed with an axially symmetric diffusion tensor model based on the D_{ratio} value from the *quadric_diffusion* analysis.[31] After the final rounds of optimization of the dynamic parameters, the D_{ratio} value was optimized to 1.13 for the NP4 complex at pH 7.3, with a τ_m of 9.36 ns.

Of 126 residues, only six residues (three outside the 13 Å excluded zone) were best fit by model 1, indicating no significant contribution from R_{ex} and local fast motions to the overall backbone relaxation. The order parameter S^2 could be fit with no time dependence ($\tau_f = \tau_s = 0$, where τ_f represents picosecond and τ_s represents nanosecond time scale motions). This is a dramatic difference from the case for NP2-NO at pH 7.3, where 110 of 128 residues were best fit by model 1.[25]

A total of 120 residues needed higher models to fit their relaxation data. Two residues (both outside the 13 Å excluded zone) were best fit by model 2, which requires τ_e (= τ_f = 100−200 ps) in addition to S^2. Another set of 91 residues (64 outside the 13 Å excluded zone) were best fit by model 3, which requires S^2 and R_{ex}. A set of 23 residues were best fit by model 4

DOI: 10.1021/bi501305a
Biochemistry 2015, 54, 221−239

(20 outside the 13 Å excluded zone), which requires S^2, R_{ex}, and τ_e ($=\tau_f$). Four residues were best fit to model 5 (two outside the 13 Å excluded zone), which requires S^2, S_f^2, and τ_e ($=\tau_s$).[31,50] Three residues were not assigned to a model. Thus, contributions from local motion and R_{ex} to the backbone relaxation occur for these 120 residues. The 120 residues are located in the loop regions as well as the eight β-strands, including residues L31, D35, and K38 located in the A−B loop and residues G126, K128, and L130 located in the G−H loop; all of these residues are within the 13 Å excluded zone. The S^2 values provide good information about the amplitude of picosecond to nanosecond local motions.[31] The typical order parameter observed in the structured regions of well-folded proteins is between 0.80 and 0.90 with an average value of 0.85 and is lower for flexible regions.[80] For NP4(sym) at pH 7.3, the average S^2 value was found to be 0.83 ± 0.04 (0.82 ± 0.03 for those outside the 13 Å excluded zone).

The *quadric_diffusion* analysis using the R_2/R_1 ratio at pH 6.5 yielded an initial estimate of the overall molecular correlation time (τ_m) of 9.4 ns with a D_{ratio} ($D_{\parallel}/D_{\perp}$) value of 1.08. After the final rounds of optimization of the dynamic parameters, the D_{ratio} value was optimized to 1.073, with a τ_m of 9.35 ns. In contrast to the pH 7.3 results, the 0.8 mM sample at pH 6.5 showed that 23 (nine outside the 13 Å excluded zone) residues were best fit with model 1, rather than only six at pH 7.3, while 92 (75 outside the 13 Å excluded zone) needed higher models to fit the experimental relaxation parameters, as compared to the case at pH 7.3, where 120 needed higher models. The squared order parameters (S^2) for the two pH high-concentration conditions are shown in Figure 5, and the

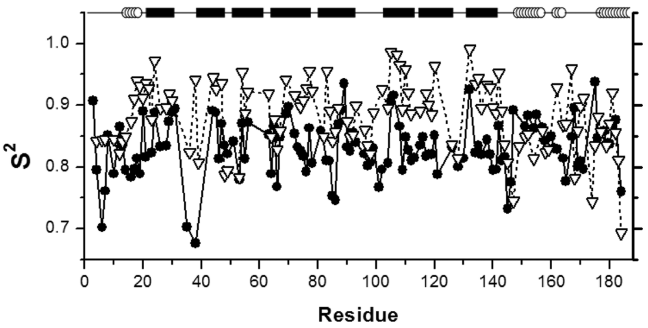

Figure 5. Calculated model-free order parameters (S^2) of high-spin NP4(sym) measured at pH 7.3 and 1.0 mM (●) and pH 6.5 and 0.8 mM (▽). The model-free order parameters were obtained by fitting the raw data to the Lipari−Szabo model-free formalism using FAST-Modelfree, as described in Materials and Methods. The locations of β-sheets and helices are shown above the plot. Note that in almost all cases, the order parameters are smaller at pH 7.3 than at pH 6.5, indicating that there is a nearly global increase in the flexibility of the residues of NP4 at physiological pH.

model assigned for each residue is shown in Table S6 of the Supporting Information for the data at pH 7.3, Table S7 of the Supporting Information for the data at pH 6.5 and 0.8 mM, and Table S8 of the Supporting Information for the data at pH 6.5 and 0.2 mM. A summary of these data at pH 7.3 and 6.5 and a concentration of 0.8 mM is given in Table S9 of the Supporting Information.

The average order parameter (S^2) values calculated from the T_1, T_2, and *NOE* data using the Modelfree approach for the various secondary structure elements at pH 7.3 and 6.5 are listed in Table 1. In most cases, it is clear that the protein is more flexible at pH 7.3 than at pH 6.5. The largest changes in S^2 occur for the A−B loop and three of the β-strands, a decrease in S^2 of 0.10 (see the change column). Unfortunately, the 0.2 mM sample did not give meaningful results, and thus, we are unable to verify whether there may some contribution from monomer−dimer exchange at pH 6.5.

The S^2 values for NP4(sym) at pH 7.3 show significant dynamics for both the loops and the β-sheets. Most importantly, the A−B loop, which is believed to be involved in the NO binding−release mechanism,[11,19] is shown to be flexible at pH 7.3, but much less so at pH 6.5, with the change in S^2 with an increase in pH from 6.5 to 7.3 being −0.10. It is interesting to note that three of the β-strands, F−H, also show a change in S^2 with an increase in pH from 6.5 to 7.3 of −0.10 or −0.09, indicating that there is significant dynamics of the β-barrel itself at pH 7.3.

The G−H loop, which is also believed to be involved in NO release,[11] does not show any of the trends seen for the A−B loop. Residues G126, N127, K128, D129, L130, G131, and D132 are in the G−H loop. Only four residues of that loop were assigned (G126, K128, L130, and D132) at pH 7.3, but only the first two could be assigned at pH 6.5. At pH 6.5, model 5 was needed for G126 and K128, while at pH 7.3, model 4 was needed for G126 and K128 and model 3 was needed for L130 and D132, suggesting a contribution of local motion and conformational exchange for these residues at pH 7.3.

Even the α-helices show some motion; helix α_1 becomes much more flexible when the pH is increased from 6.5 to 7.3 (change in S^2 of −0.07), while the residues of helices α_2 and α_3 show increased rigidity (S^2 changes of +0.04 and +0.02, respectively), with the residues behaving mainly according to model 3. At pH 6.5, the 0.8 mM sample behaves mainly according to model 2 for helix α_1, but mainly according to model 5 for helices α_2 and α_3. The very short helices, α_2' and α_2'', however, both show changes in S^2 of −0.04, showing increased flexibility at pH 7.3, in line with the behavior of most of the other secondary structure elements.

The S^2 values for all residues in the structured regions, namely, β-sheets and α-helices, are near the 0.83 average at pH 7.3 and 0.82 for the 13 Å excluded zone, indicating the fairly high rigidity of the molecule; a total of 27 (23 outside the 13 Å excluded zone) residues had S^2 values one standard deviation greater than the average. Many of the residues in the loop regions, with some exceptions, show values of S^2 of <0.80, suggesting that most of the loop regions are flexible. At pH 7.3, a total of 28 residues (K4, A6, I7, T10, K14, D16, Y17, N19, D35, K38, L53, T64, D66, V76, N85, F86, A101, G102, Y104, V109, T121, N140, K141, A145, G146, S165, C171, and K184) have S^2 values of <0.80, indicating that those residues are more flexible than others. It is interesting to note that three residues in the A−B loop (L31, D35, and K38) show flexibility but unlikely correlated motion, but there is no evidence of any correlated motion in the G−H loop, where only four residues were assigned at pH 7.3. At pH 6.5 for the 0.8 mM sample, where the overall average value of S^2 is 0.88 ± 0.05, 18 residues have S^2 values one standard deviation lower (F12, V36, R39, T48, A49, S53, D66, A98, K128, A145, D147, S154, L158, E159, E168, D174, T183, and K184). The underlined residues are near the end or beginning of a β-strand or α-helix, while all the others are in loops. Only three of these residues (V36, R39, and D66) are within the 13 Å excluded zone.

It is noteworthy that the resonances of the A−B and G−H loop regions of the protein showed pH-dependent perturbation

DOI: 10.1021/bi501305a
Biochemistry 2015, 54, 221−239

Table 1. Average Modelfree Order Parameter Values for NP4 Secondary Structure Elements

		pH 6.5, 0.8 mM		pH 7.3, 1.0 mM	CPMG, pH 6.5, 0.8 mM			CPMG, pH 7.3		
structure	NP4 residues	S^2 (no. of data)	change	S^2 (no. of data)	model 1	model 2	model 3	model 1	model 2	model 3
helix										
α_1	13−18	0.88 ± 0.04 (5)	−0.07	0.81 ± 0.01 (5)	5	1	0	6	0	0
α_2	146−156	0.82 ± 0.03 (5)	+0.04	0.86 ± 0.03 (5)	10	0	0	9	0	0
α_2'	159−163	0.88 ± 0.05 (2)	−0.04	0.84 ± 0.01 (3)	5	0	0	3	0	0
α_2''	167−170	0.88 ± 0.05 (4)	−0.04	0.84 ± 0.02 (4)	2	1	1	1	0	1
α_3	174−182	0.85 ± 0.03 (8)	+0.02	0.87 ± 0.02 (7)	6	1	0	7	0	2
strand										
β_A	19−30	0.92 ± 0.02 (10)	−0.07	0.85 ± 0.03 (9)	6	2	4	4	0	6
β_B	41−49	0.88 ± 0.07 (4)	−0.03	0.85 ± 0.03 (6)	0	5	1	4	0	2
β_C	52−60	0.89 ± 0.05 (4)	−0.06	0.83 ± 0.04 (4)	2	1	1	2	0	4
β_D	67−78	0.92 ± 0.02 (8)	−0.08	0.84 ± 0.03 (10)	0	2	2	1	2	7
β_E	81−89	0.88 ± 0.03 (6)	−0.03	0.85 ± 0.06 (8)	3	4	0	3	1	5
β_F	103−112	0.94 ± 0.04 (8)	−0.09	0.85 ± 0.04 (8)	4	0	2	4	0	5
β_G	116−125	0.92 ± 0.02 (4)	−0.10	0.82 ± 0.02 (6)	4	1	1	2	3	2
β_H	133−138	0.93 ± 0.02 (4)	−0.10	0.83 ± 0.01 (4)	1	1	1	0	0	4
linker										
T3−α_1	3−12	0.84 ± 0.01 (6)	−0.03	0.80 ± 0.05 (6)	5	1	1	5	1	0
α_2−α_2'	157 and 158	0.84 ± 0.02 (3)	−0.03	0.85 ± 0.01 (2)	2	0	0	2	0	0
α_2'−α_2''	164−166	0.87 ± 0.00 (2)	−0.07	0.80 ± 0.02 (2)	2	0	0	0	1	1
α_2''−α_3	171−173	0.91 (1)	−	0.80 (1)	0	1	0	2	0	0
α_3−end	183 and 184	0.75 ± 0.06 (2)	−	0.76 (1)	2	0	0	2	0	0
reverse turn										
β_A−β_B	31−40	0.86 ± 0.06 (5)	−0.10	0.76 ± 0.09 (3)	2	1	1	3	1	1
β_B−β_C	50 and 51	0.79 (1)	+0.05	0.84 (1)	0	0	1	0	0	0
β_C−β_D	61−66	0.87 ± 0.03 (4)	−0.03	0.82 ± 0.04 (4)	3	0	0	3	0	1
β_D−β_E	79 and 80	− (0)	−	− (0)	0	0	0	1	0	0
β_E−β_F	90−102	0.87 ± 0.03 (9)	−0.03	0.82 ± 0.02 (10)	7	0	0	7	3	1
β_F−β_G	113−115	0.89 (1)	−0.06	0.83 ± 0.01 (2)	3	0	0	3	0	0
β_G−β_H	126−132	0.88 ± 0.07 (3)	−0.04	0.84 ± 0.04 (4)	0	1	3	0	2	4
β_H−α_2	139−145	0.89 ± 0.04 (7)	−0.08	0.81 ± 0.03 (7)	2	4	1	2	5	0

of their chemical shifts, as discussed above and shown in Figure 3. The R_1, R_2, and NOE values for NP4(sym) measured at pH 7.3 are shown in Figure 4. The R_1 values for most of the residues fall within the range of the average value of all residues. At pH 7.3, the average R_1 is 1.24 ± 0.06 s^{-1}; 12 residues have R_1 values of one standard deviation less than this value, as summarized in Table S3 of the Supporting Information. At pH 6.5, the average R_1 is 1.55 ± 0.08 s^{-1} at 0.2 mM and 1.45 ± 0.08 s^{-1} at 0.8 mM. Similarly, the R_2 values for most residues fall within reasonable range of the average value for all residues, as summarized in Table S4 of the Supporting Information. A similar analysis of the $^{15}N\{^1H\}$ NOEs shows that at pH 7.3, the average |NOE| is 0.79 ± 0.06, as summarized in Table S5 of the Supporting Information. An overall summary is provided in Table 2.

The R_{ex} values calculated for those residues that exhibit model 3 or model 4 behavior are shown as a function of residue number in Figure 6 for pH 7.3 and 1.0 mM and for pH 6.5 and 0.8 mM. At pH 7.3, there are 90 residues that show model 3 behavior (64 outside the 13 Å zone). The average R_{ex} is 2.5 rad s^{-1} (2.2 rad s^{-1} for those outside the 13 Å zone), and the range extends from 0.1 to 14.4 rad s^{-1} (the range is the same for those outside the 13 Å zone). There are 22 (20 outside the 13 Å zone) residues that show model 4 behavior at pH 7.3. The average R_{ex} for these model 4 residues is 2.4 rad s^{-1} (2.2 rad s^{-1} for those outside the 13 Å zone), and the range extends from 0.5 to 4.8 rad s^{-1} (the range is the same for those outside the 13 Å zone). For the 0.8 mM data at pH 6.5, there are 19 residues that show model 3 behavior (nine outside the 13 Å excluded zone). The average R_{ex} value for the pH 6.5, 0.8 mM model 3 residues is 2.5 rad s^{-1} (2.0 rad s^{-1} for those outside the 13 Å excluded zone), and the range extends from 0.3 to 12.6 rad s^{-1} (from 0.3 to 3.9 rad s^{-1} for the nine outside the 13 Å excluded zone). There are 24 model 4 residues for the 0.8 mM data at pH 6.5 (19 outside the 13 Å excluded zone). The average R_{ex} for these residues is 2.1 rad s^{-1} (2.0 rad s^{-1} for those outside the 13 Å excluded zone), with a range of 0.2−7.5 rad s^{-1} (0.2−6.0 rad s^{-1} for those outside the 13 Å excluded zone).

The τ_e values of residues that exhibit behavior of models 2, 4, and 5 are included in Tables S6−S8 of the Supporting Information. At pH 7.3, there are two residues (both outside the 13 Å excluded zone) that show model 2 behavior with an average τ_e of 25 ps, there are 24 residues (20 outside the 13 Å excluded zone) that show model 4 behavior with an average τ_e of 20 ps (21 ps for those outside the 13 Å excluded zone), and there are four residues (two outside the 13 Å excluded zone) that show model 5 behavior with an average τ_e of 0.75 ns (0.87 ns for those outside the 13 Å excluded zone). This major difference in the average τ_e value for model 5 residues is to be expected, because model 5 represents the residues with slower motions, where $\tau_e = \tau_s$.[31,50] However, these τ_e values are still shorter than the τ_m value of 9.36 ns and thus do represent motions of a small part of the molecule that are faster than the rotational tumbling time of the molecule as a whole.

At pH 6.5 and 0.8 mM, there are 10 residues that show model 2 behavior with one outlier (nine outside the 13 Å

DOI: 10.1021/bi501305a
Biochemistry 2015, 54, 221−239

Table 2. Statistics of Backbone Dynamics of High-Spin NP4-OH_2 as a Function of pH, As Compared to Those of NP2-NO[25] and High-Spin NP2-OH_2 at pH 7.3[a]

	pH 6.5	pH 7.3	NP2-NO, pH 7.3[25] (HS NP2, pH 7.3, CPMG only)*
R_1 (s^{-1}) average (0.8 mM)	1.55 ± 0.08	1.24 ± 0.06	1.45 ± 0.10
no. of $R_1 \leq 1$ STD smaller	55(132)	12(131)	
R_1 (s^{-1}) average (0.2 mM)	1.45 ± 0.08		
no. of $R_1 \leq 1$ STD smaller	53(132)		
R_2 (s^{-1}) average (0.8 mM)	13.5 ± 1.5	13.8 ± 1.4	12.0 ± 2.87
no. of $R_2 \geq 1$ STD larger	17(132)	12(131)	
R_2 (s^{-1}) average (0.2 mM)	12.3 ± 1.5 s^{-1}		
no. of $R_2 \geq 1$ STD larger	12(132)		
$^{15}N\{^1H\}$ NOE average (0.8 mM)	0.78 ± 0.04	0.79 ± 0.06	0.78 ± 0.10
no. of NOE ≥ 1 STD larger	36(132)	27(131)	
$^{15}N\{^1H\}$ NOE average (0.2 mM)	0.79 ± 0.04		
no. of NOE ≥ 1 STD larger	30(132)		
S^2 (0.8 mM)	0.88 ± 0.04	0.83 ± 0.04	0.87 ± 0.06
no. of $S^2 \geq 1$ STD	30(80)	27(126)	
S^2 (0.2 mM)	0.87 ± 0.07		
no. of $S^2 \geq 1$ STD	13(60)		
	Number of Residues in Each Model-Free Model		
model 1 (S^2) (0.8 mM)	23	6	109
model 1 (S^2) (0.2 mM)	6		
model 2 (S^2, τ_e) (0.8 mM)	11	2	17
average τ_e (ps)	33	25	
model 2 (S^2, τ_e) (0.2 mM)	7		
average τ_e (ps)	1452		
model 3 (S^2, R_{ex}) (0.8 mM)	17	91	8
average R_{ex} (rad s^{-1})	2.5	2.4	
0.2 mM	10		
average R_{ex} (rad s^{-1})	171		
model 4 (S^2, R_{ex}, τ_e) (0.8 mM)	23(19)	23	7
average R_{ex} (rad s^{-1})	2.1	2.4	
average τ_e (ps)	50	20	
model 4 (S^2, R_{ex}, τ_e) (0.2 mM)	3		
average R_{ex} (rad s^{-1})	2.7		
average τ_e (ps)	690		
model 5 (S^2, S_f^2, τ_e) (0.8 mM)	41	4	3
average τ_e (ns)	2.1	0.7	
model 5 (S^2, S_f^2, τ_e) (0.2 mM)	13		
average τ_e (ns)	3.2		
unassigned model (0.8 mM)	15	3	1
0.2 mM	50		
prolines, no. of overlapped and unassigned peaks	54	55	34

DOI: 10.1021/bi501305a
Biochemistry 2015, 54, 221−239

Table 2. continued

	pH 6.5	pH 7.3	NP2-NO, pH 7.3[25] (HS NP2, pH 7.3, CPMG only)*
	Relaxation Dispersion Parameters [high $\Delta R_2^{\text{eff}}(\nu_{\text{CPMG}})$]		
model 1	77	73	89
(no R_{ex})			(107)
model 2			
(R_{ex}, k_{ex}; $k_{\text{ex}} \ll \delta\omega$)	28	17	up to 4[b]
	I7, Y17, V22, Y28, D34, A45, A46, G47, T48, A49, E55, S72, Q75, Y82, T83, A84, N85, V99, K125, G126, L137, N140, D142, A143, A145, N169, C171, L182	I7, D34, T67, L74, N85, K91, N92, V99, A117, L118, K125, N140, K141, D142, A143, A145, S165	(up to 20)[b,c]
model 3	24	44	up to 4[b]
(R_{ex}, k_{ex}; $k_{\text{ex}} \gg \delta\omega$)	T3, G20, W23, Y24, L29, K38, L44, G51, K54, Y69, L74, G80, T100, A101, G102, V109, M110, A117, K128, D129, D132, V136, K141, N170	Y24, T26, D27, Y28, L29, D30, L31, E32, K38, L44, G47, K54, E55, A56, D66, Y69, V71, S72, Q75, V76, E77, S78, T83, A84, F86, K87, K88, T100, N103, Y104, T106, F107, I119, G126, K128, L130, D132, A135, V136, N138, I164, K167, S177, L178	(up to 20)[b,c]
no. of backbone ^{15}N atoms within 10 Å of Fe	4	5	N/A[d]
			(up to 20)[c]
unknown	51	47	84[b]
			(52 or more)[c]

[a]This work. [b]These were two-point CPMG measurements: $\Delta R_2^{\text{eff}}(\nu_{\text{CPMG}}) = (1/T_{\text{cp}}) \ln(I_{1000}/I_{50})$ (eq 1), where I_{1000} and I_{50} are the heights of cross-peaks in spectra collected at effective CPMG fields of 1000 and 50 Hz, respectively, and T_{cp} is the constant time delay (0.06 s). Because models are not assigned in the two-point treatment, those residues that show motion could be of either model 2 or model 3; thus, the number given is actually the sum of potential model 2 and model 3 residues. [c]These are for the high-spin NP2 data, where peaks were not assigned. Thus, we do not know whether all of the possible residues within 10 Å of Fe could have been assigned. Those that could not be assigned will be subtracted from the 20 possible and added to unknown. [d]NP2-NO is diamagnetic, so there is no reason to consider residues only outside of 10 Å or any other distance from Fe.

DOI: 10.1021/bi501305a
Biochemistry 2015, 54, 221−239

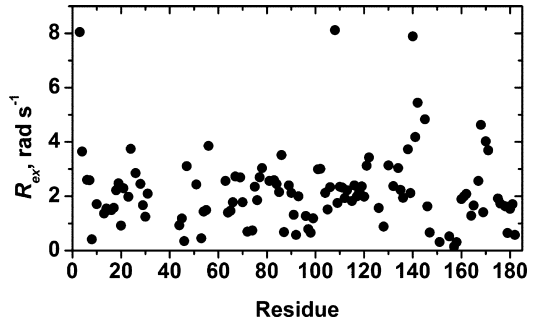

Figure 6. Apparent contribution to transverse relaxation (R_{ex}) from chemical exchange in high-spin NP4(sym) at pH 7.3 and 1.0 mM obtained from the Modelfree analysis. The overall average value for R_{ex} is 2.5 rad s^{-1} (2.2 rad s^{-1} for those outside the 13 Å zone). The largest value (14.5 rad s^{-1}) is not shown.

excluded zone) with an average τ_e of 34 ps (one residue has a very large τ_e value of 1897 ps and was not included in the average), there are 19 residues that show model 4 behavior with an average τ_e of 40 ps, and 41 residues (38 outside the 13 Å excluded zone) show model 5 behavior with an average τ_e of 2.1 ns. The values of τ_e obtained for the 0.2 mM sample at pH 6.5 for models 2, 4, and 5 are far different (all nanosecond values) from those obtained from the 0.8 mM sample at pH 6.5 or the 1.0 mM sample at pH 7.3 (picosecond values for models 2 and 4 and nanosecond values for model 5, as expected). Careful analysis of the data shows that the 0.2 mM sample is simply too dilute to provide reasonable statistics. The fact that 50 residues could not be assigned a model, and that of those that were assigned a model, 16 had S^2 values of 1.0 (Table 2), and thus could not be included in the results, shows clearly that with an increase in the number of scans of a factor of only 2, the artifacts created by the low concentration of this sample preclude taking the results obtained seriously. Because of this conclusion regarding the 0.2 mM data, we cannot be certain that the 0.8 mM data at pH 6.5 have no contribution to the results from the monomer−dimer equilibrium. However, the larger number (34 vs 25) of residues having picosecond motions at pH 6.5 and 0.8 mM than at pH 7.3 raises the possibility that the pH 6.5 data may have contributions from the monomer−dimer equilibrium.

Slow Time Scale Dynamics. Transverse relaxation (R_2) measurements using the Carr−Purcell−Meiboom−Gill (CPMG) pulse sequence have emerged as a very powerful method for studying the slow time scale motions (microseconds to milliseconds) in protein dynamics.[35,36] To probe backbone motions of the NP4 complex occurring on these slow time scales, effective transverse ^{15}N relaxation rates (R_2^{eff}) were recorded as a function of CPMG field strength (ν_{CPMG}) at pH 7.3, and at pH 6.5 at two concentrations, 0.8 and 0.02 mM. R_2 values were larger at the higher concentration without exception, as expected because of the difference in viscosity at the two protein concentrations. The data were analyzed using NESSY.[73] NESSY divides the motions on the microsecond to millisecond time scales into three models. Model 1 is for residues that show no time-dependent relaxation behavior ($R_2^{eff} = R_2^0$), while models 2 and 3 are for residues that show time-dependent relaxation behavior in which R_2^{eff} is assumed to behave according to slow-limit exchange between the two sites ($k_{ex} \ll \delta\omega$) for model 2 and fast-limit exchange between the two sites ($k_{ex} \gg \delta\omega$) for model 3, where $\delta\omega$ is the frequency difference between the two signals for a given residue.[73]

In analyzing the CPMG data, we assumed that the two concentrations (0.8 and 0.2 mM) at pH 6.5 should behave according to the same model for a given residue and should have similar values of k_{ex}. We eliminated residues whose ^{15}N atoms were within 13 Å of iron (35 at pH 7.5 and 24 at pH 6.5) and those that could not be assigned or whose peak was overlapped with that of another residue, a combined total of 81 at pH 7.3 and 78 at pH 6.5. At pH 7.3, the program found best fits for 73 residues (70 outside the 13 Å excluded zone) as model 1, meaning R_2^{eff} values are not dependent on the CPMG field for those residues, while at pH 6.5, the number of residues found to be model 1 decreases to 77 (67 outside the 13 Å excluded zone). The dispersion curves for those residues were

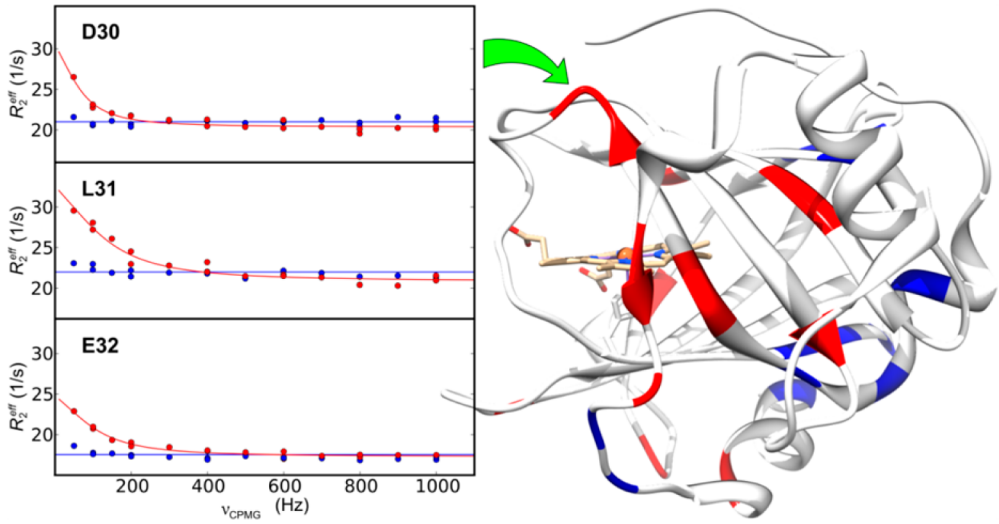

Figure 7. Transverse relaxation dispersions (left) of the backbone ^{15}N nuclei, at pH 7.3 (red) and pH 6.5 (blue), of residues D30, L31, and E32, the latter two of which are part of the A−B loop, indicated with the green arrow on the NP4(sym) structure. All three of these residues were found to be fit to model 3. The numerical values of k_{ex} are 456, 885, and 722 s^{-1} at pH 7.3, respectively. Changes in the model assignments (right) that occur on pH change, mapped onto the ribbon diagram of the NP4(sym) structure (PDB entry 3C78), with red indicating model 1 assignment at pH 6.5 changes to model 2 or 3 at pH 7.3 and blue indicating the reverse change. Helix α_2 is where most of the increased rigidity at pH 7.3 is seen.

DOI: 10.1021/bi501305a
Biochemistry 2015, 54, 221−239

flat: there were no CPMG field-dependent peak intensity changes observed. At pH 7.3, the program found best fits for 17 residues as model 2 (15 outside the 13 Å excluded zone), while at pH 6.5, that number increased to 28 (22 outside the 13 Å excluded zone), meaning in both cases that k_{ex} and R_{ex} could be calculated. At pH 7.3, the program found best fits for 44 residues as model 3 (18 of which were outside the 13 Å excluded zone), and at pH 6.5, 24 residues (17 outside of the 13 Å excluded zone) were best fit by model 3, meaning that for NP4 there are considerable dynamics on the micro- to millisecond time scales at both pH values. When the results are compared, the majority showed the same model at both pH values. Examples of the results for D30, L31, and E32 of the A−B loop are shown in Figure 7. The CPMG results, in terms of the model that best fit the time-dependent data for each of the secondary structure elements, are included in Table 2, and the individual R_2^{eff} plots for each residue are shown in Figures S7 (pH 6.5 vs pH 7.3) and S8 (pH 6.5, 0.8 mM vs 0.2 mM) of the Supporting Information.

There were two types of exceptions to the general finding that the majority of residues show the same model at both pH values: those that showed model 1 at the lower pH and model 2 or 3 at the higher and those that showed the opposite, model 2 or 3 at the lower pH and model 1 at the higher. The first exception is easy to understand, where a rigid residue at the lower pH shows more dynamics at the higher pH; residues in this group include T26, D27, Y28, D30, L31, E32, D66, K91, N103, Y104, L118, I119, I164, S165, K167, and S177. Residues that show the opposite, rigidity (model 1) at the higher pH but dynamics (model 2 or 3) at the lower pH, include Y17, G20, W23, A45, A46, T48, A49, G80, Y82, V109, M110, N169, C171, and L182. Another case is that in which at pH 6.5 the residue shows model 2 (slow limit) behavior while at pH 7.3 it shows model 3 (fast limit) behavior (G47, E55, S72, Q75, T83, A84, and G126). The opposite, where the residue shows model 3 (fast limit) behavior at pH 6.5 while at pH 7.3 it shows model 2 (slow limit) behavior (L74, A117, and K141), is more difficult to understand, and this occurs less frequently. However, because the resonances may have moved between pH 7.3 and 6.5, it could be the difference in $\delta\omega$ at the two pH values that changes the model. The results are shown in the right panel of Figure 7 in terms of the color of each residue. Most residues in the A−B and G−H loops could be analyzed; however, in many cases, their data did not provide good fits, and two of the residues in the A−B loop are prolines. At pH 7.3, L31, E32, and K38 of the A−B loop and G126, K128, L130, and D132 of the G−H loop require model 3 (fast exchange) to fit their CPMG data, whereas D34 is best fit by model 2 (slow exchange) and D35 by model 1. It is interesting to note that of A−B loop residues, L31 and E32 are rigid at pH 6.5 on the micro- to millisecond time scale, but at pH 7.3 L31 and E32 are mobile on the micro- to millisecond time scale, as L31 is with Modelfree analysis at the same pH. K38 is mobile at both pH values on the micro- to millisecond time scale at pH 7.3, but not at pH 6.5 with Modelfree analysis, thus showing motions on the fast time scales, and also evidence of micro- to millisecond conformational exchange. Some of the residues that best fit model 3 at pH 7.3 were best fit to model 1 at pH 6.5, suggesting that they became more rigid as the pH was decreased. The only exceptions were D34 and K38, which maintained their same model (2) when the pH was decreased to 6.5. For the G−H loop at pH 6.5, K128, D129, and L130 best fit model 3 (fast exchange), while G126 best fits model 2 (slow exchange). Modelfree analysis showed G126 and K128 to have a R_{ex} component to their fast time scale motions at pH 6.5, while G126, K128, L130, and D132 all have a R_{ex} component at pH 7.3.

The differences in k_{ex} for residues that fit to model 2 or model 3 of the CPMG data at pH 7.3 are summarized as follows. There are 17 model 2 residues, whose average k_{ex} is 2062 s^{-1}, but the range extends from 502 to 8397 s^{-1} (and we do not expect the average to be exhibited by all residues, because their motions are clearly not correlated). There are 48 model 3 residues, four of which have errors larger than the value of k_{ex}. Apart from those four, the 44 values of k_{ex} yield an average of 977 s^{-1}, with a range of 372−3000 s^{-1} (for the 17 that are >13 Å from Fe, the average k_{ex} is 1083 s^{-1} with a range of 502−2873 s^{-1}). The differences in k_{ex} for residues that fit to model 2 or model 3 at the higher protein concentration at pH 6.5 are summarized as follows. At 0.8 mM, there are 28 model 2 residues (22 of which are outside the 13 Å excluded zone), whose average k_{ex} is 1303 s^{-1}, with a range of 316−6140 s^{-1} (for the 22 the average is 1492 s^{-1}, with the same range). At the same concentration, there are 24 model 3 residues, six of which have errors larger than the number. For the 18, the average k_{ex} is 748 s^{-1}, with a range of 25−3000 s^{-1}. Thus, at pH 6.5, the 0.8 mM sample shows fewer model 2 and 3 residues than are seen at pH 7.5, and thus, there is no obvious evidence of monomer−dimer equilibria in the CPMG data. All of the CPMG results are summarized in Table 2.

The residues that are found to fit to model 2 or 3 for the CPMG experiments, and thus show micro- to millisecond dynamics, are in general not scattered, but they are also not all in loops; it seems that the ends or beginnings of β-sheets, as well as loops, are involved in these dynamics, whereas helices were invariably best fit by model 1 (residues F12−F18, G146−F163, and D174−L182, with few exceptions). Examples of parts of β-strands that show model 2 or 3 behavior are the second half of β_A and most of the A−B loop, two residues of β_B and parts of β_C−β_F, a part of the E−F loop, part of β_G and β_H, and the four residues of the G−H loop that have been analyzed. However, k_{ex} and R_{ex} values observed for neighboring residues are quite different from each other, suggesting that motions are not correlated.

Summary of High-Spin Native N-Terminal NP2 Fast and Slow Time Scale Data at pH 7.3. All of the experiments for the Modelfree analysis were conducted at pH 7.3 for high-spin native N-terminal NP2-OH_2, but upon preliminary analysis of the data, it became clear that although high-spin NP2 shows more dynamics than did diamagnetic native N-terminus NP2-NO,[25] it showed significantly less than NP4-OH_2. The R_1, R_2, and NOE values of the ^{15}N-labeled high-spin NP2 sample at pH 7.3 are plotted in Figure 8. In comparison to the results for NP4(sym) at pH 7.3, the R_1, R_2, and NOE values for all the residues of NP2 are much closer in range to the average values, with few exceptions. None of the residues showed time-dependent decay curves for R_1, R_2, or NOE. The R_1, R_2, and NOE data are summarized by peak numbers in Table 13 of the Supporting Information. Only ∼18 residues of high-spin NP2 could be assigned confidently on the basis of the assignments made at pH 7.3 for the diamagnetic NP2-NO sample,[25] because the ^{15}N chemical shifts are similar (within ∼0.2 ppm) in the two spin states, while the ^{1}H chemical shifts differ by somewhat more (∼0.4 ppm). Because the 18 residues that were readily assigned are scattered throughout the protein, with only one in the A−B loop and none in the G−H loop, the assigned residues

DOI: 10.1021/bi501305a
Biochemistry 2015, 54, 221−239

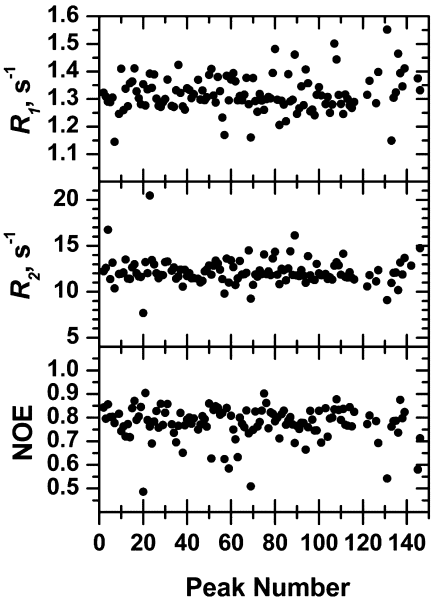

Figure 8. R_1, R_2, and NOE values of high-spin native N-terminal NP2 measured at pH 7.3 and 30 °C. Because backbone assignments were not made, peak numbers are used. Few significant increases in R_2 above the average value observed for all the peaks are observed, indicating very little conformational exchange contribution to the relaxation on the pico- to nanosecond time scale.

are not much help in understanding the dynamics of NP2. The full plots of all peaks that were observed are shown in Figure 9

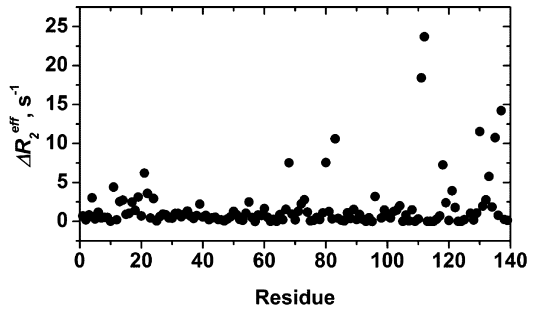

Figure 9. Per residue plot of $\Delta R_2^{eff}(\nu_{CPMG})$ for high-spin native N-terminal NP2 at pH 7.3 and 30 °C, showing motions on the micro- to millisecond time scale at pH 7.3 as a function of peak number. Approximately 20 residues show evidence of motions on the micro- to millisecond time scales. More than four residues were found for NP2-NO at pH 7.3.[25]

for the ΔR_2^{eff} from the CPMG experiment, also measured at pH 7.3 and 30 °C. The ΔR_2^{eff} data were obtained from two-point measurements described by eq 1 in Relaxation Dispersion Analysis of NP4 Data at pH 7.3 and 6.5 and NP2 Data at pH 7.3. As can be seen, the high-spin protein is slightly less rigid than NP2-NO[25] but much more rigid than NP4(sym). Therefore, it was deemed a poor investment of time to assign all of the resonances of high-spin NP2 at pH 7.3. Thus, the native N-terminal NP2 CPMG results are listed as peak numbers in Table 14 of the Supporting Information. The results for high-spin native N-terminal NP2 are included in Table 2.

DISCUSSION

NP4(sym) exhibits extensive dynamics at pH 7.3, the pH of human tissues, where NO is expected to dissociate from the protein, travel through cell walls, and reach the capillaries to cause vasodilation, thereby bringing more blood to the region and allowing the insect to obtain a sufficient blood meal in a short time period. In comparison, at pH 6.5, which is much higher than that of the insect's saliva, it shows much less dynamics, and a global look at the behavior of secondary structure elements (Table 1) shows that there are significant changes in the order parameters of these secondary structure elements as the pH is increased from 6.5 to 7.3. Compared to other lipocalins, including the 10-stranded β-barrel human bile binding protein studied recently by Toke and co-workers,[50] NP4 shows significantly more dynamics at both pH 6.5 and 7.3. The bile binding protein shows a much larger number of residues (84 for apo and 85 for holo) to have model 1 behavior and many fewer (11, 11, 0, and 8 for apo vs 11, 9, 0, and 9 for holo) residues showing model 2−5 behavior, respectively, with three apo residues and one holo residue, respectively, not being assigned to a model.[50] In that protein, 10 apo versus 11 holo residues showed fast time scale motions ranging from 37 to 132 ps (apo) versus 28 to 112 ps (holo), and nine showed motions ranging from 1.4 to 4.9 ns (apo) and nine holoprotein residues motions ranging from 0.7 to 6.7 ns. The bile binding protein had an overall rotational correlation time of 6.8 ns, and the $D_{\|}/D_{\perp}$ values of the apoprotein and holoprotein differed significantly (1.13 and 0.88, respectively).[50]

In comparison to other types of proteins, high-spin NP4(sym) shows somewhat more dynamics than the Src phosphopeptide-complexed homology 2 domain studied by Kay and co-workers,[29] which is only ∼80 residues in size and consists of six β-strands and two α-helices and has 29, 10, 20, 5, and 7 model 1−5 residues, respectively, with nine residues not assigned to a model. Doubling those numbers would be a more direct comparison to NP4, which still shows that NP4(sym) has an extremely large number of residues (91) that behave according to model 3 at pH 7.3 and are thus sensitive to S^2 and R_{ex}. In comparison, the study of interleukin 1β, a 153-residue protein consisting of 12 β-strands and two short helices, by Clore and co-workers,[29] showed that 128 of a total of 144 assignable residues showed motions on the 20−50 ps time scale and 32 showed motions on the 0.5−4 ns time scale; the overall rotational correlation time was 8.3 ns, whereas for NP4(sym), we see that there are 25 residues of the 124 that could be used for Modelfree analysis that have motions on the 11−46 ps time scale and three residues that have motion on the 0.5−1 ns time scale at pH 7.3 but 27 residues of the 124 that have motions on the 4−82 ps time scale and 46 on the 0.15−5.2 ns time scale at pH 6.5 and 0.8 mM. At both pH values, the overall rotational correlation time of NP4(sym) was 9.4 ns. Thus, while slightly larger than interleukin 1β, NP4(sym) is not as flexible. Finally, *Escherichia coli* ribonuclease H is an α/β protein of 155 residues that has been studied by the Palmer group.[31] Model-free analysis of 116 assigned residues of RNase H showed that 65 residues behave according to model 1, nine according to model 2, 29 according to model 3, two according to model 4, and nine according to model 5. Ten residues have motions on the 28−84 ps time scale, and nine have motions on the 0.7−4.5 ns time scale. The global rotational correlation time was found to be 9.69 ns. This is a profile similar to that of the Src phosphopeptide-complexed homology 2 domain studied by

DOI: 10.1021/bi501305a
Biochemistry 2015, 54, 221−239

Kay et al.,[30] and NP4(sym) at pH 7.3 also shows somewhat more dynamics than *E. coli* RNase H.[31]

As we can see from the results obtained in this study, NP4(sym) shows much more dynamics on all time scales at both pH 6.5 and 7.3 than does native N-terminal NP2. In fact, the differences in the amount of dynamics between NP4 and NP2 are so large that they cannot be explained simply by the presence of one more amino acid in the A−B loop of NP4 as compared to NP2. After considerable thought about what else might be different about these two seemingly very similar proteins, we have analyzed the hydrogen bonding patterns of the two proteins as one possible way in which they might differ. Both proteins lack one amino acid from a β-strand that the other protein has, actually before β_A for NP2, but at the beginning of β_E for NP4, and NP2 lacks one amino acid in the A−B loop as compared to NP4. We find that with respect to the region of the protein sequence that encompasses the eight β-strands of the β-barrel, from Tyr24 to Asn138 of NP4 and from Tyr23 to Thr137 of NP2, NP4 has a larger β-barrel than does NP2, and thus, the heme fits more loosely inside the NP4 β-barrel, which means that the NP4 protein has the possibility of more low-energy, fast dynamic motions than does NP2.

Specifically, the hydrogen bonds of backbone NH and C=O groups between β_H and β_A begin with Asn138 and Tyr24 and end with Asp132 and Leu31 for NP4 but begin with Thr137 and Tyr23 and end with Asp131 and Lys30 for NP2, as shown in Figure S6 of the Supporting Information. Because the numbering of these two β-strands goes in opposite directions, NP4 has two more amino acids in the β-barrel than does NP2. Thus, the β-barrel of NP4 at the open end has a circumference two amino acids larger than that of NP2, which could add, we estimate, up to 4−6 Å to the circumference of the β-barrel of NP4 at the open end. The result of the larger circumference for NP4 is that apo-NP4[81] and holo-NP4[15] have almost identical protein structures, with a fairly round β-barrel in each case,[81] whereas while apo-NP2 shows a similar, fairly round β-barrel,[a] holo-NP2 shows an oblong β-barrel,[9] with a width at the point where the heme lies that is at least 1.4 Å wider than that of apo-NP2; it is the β_D and β_E strands that show this at least 1.4 Å outward movement.[1] This explains the fact that the heme is much more crowded in the NP2 protein, which causes it to be much more ruffled than the heme of NP4.[10−15] This also causes it to be much more sensitive to the size of protein side chains that point toward the heme and thus cause one heme orientation to be favored over the other for NP2 (DOI: 10.1021/bi5013047) but not for NP4 (see Scheme I of the Supporting Information). The effect of this crowding due to two fewer amino acids in the β-barrel on the heme protein is to make it much more rigid, and for NP2 to show much less dynamics than NP4.

The use of the symmetrical hemin for the NP4 study may have created somewhat more dynamics for NP4, but we estimate the difference would be small. To evaluate the contribution of the two fewer atoms of the symmetrical hemin, we would need to investigate the Modelfree behavior of NP2 reconstituted with the symmetrical hemin, a very time-consuming project, which is deemed unlikely to yield markedly different results. We would also need to investigate NP4 reconstituted with protohemin, which would give two $^1H\{^{15}N\}$ HSQC peaks for each residue that is fairly close to the heme (how far, 13 Å, 15 Å, or more?), which would make the Modelfree calculations extremely difficult, and likely impossible. From available data, we know that the crystal structures of NP4(sym) (PDB entry 3C78) and NP4(protohemin) (PDB entry 1X8P) show similar ruffling of the prosthetic group, but with NP4(sym) having the very slightly more ruffled heme, again indicating that the larger β-barrel of NP4 permits greater freedom for the heme to freely adjust its structure; we have also mentioned that distances of the various amide ^{15}N atoms from the paramagnetic Fe(III) of NP4 are up to 0.15 Å smaller for the symmetrical hemin complex (PDB entry 3C78) than for the protoheme complex (PDB entry 1X8P). Unfortunately, there has been no structure reported for NP2 bound to the symmetrical hemin; however, the fact that the protohemin prosthetic group is up to twice as ruffled, as measured by the alternating out-of-plane displacements of the *meso* carbons, in NP2(protohemin) structures as compared to NP4-(protohemin) structures[b] suggests that the two fewer carbons of the symmetrical hemin as compared to protohemin might indeed make a measurable difference in the dynamics of NP2 (an increase), but for NP4, with its larger β-barrel, the two fewer carbons of the symmetrical hemin will likely make a much smaller increase in the dynamics of NP4. This is reflected in the k_d for the loss of NO from (M0)NP1(sym) at pH 7.5, which is somewhat larger (2.66 s^{-1}) than the k_d for the loss of NO from (M0)NP1(proto) (2.32 s^{-1}, a difference of a factor of 1.15), but the differences in the k_d values for NO loss at pH 7.5 from NP4(proto) and native N-terminal NP2(proto) are many times larger (1.60 and 0.093 s^{-1}, respectively, a difference of a factor of 17.2).[82] Thus, the differences between NP2 and NP4 are, in all cases, much greater than the differences between NP4 reconstituted with protohemin and NP4 reconstituted with the symmetrical hemin, 2,4-dimethyldeuterohemin, and thus, the results of this study (massively more dynamics observed for NP4 than for NP2) are meaningful.

■ ASSOCIATED CONTENT

Supporting Information

Figures showing the sequences of the four nitrophorins and some assignment details, the $^1H\{^{15}N\}$ HSQC map of NP4 at pH 7.3 with assignments, the absolute change in chemical shifts of NP4 backbone residues between pH 6.5 and 7.3, comparison of amide N−Fe distances and peak S/N in the $^1H\{^{15}N\}$ HSQC spectrum of NP4, comparison of the longitudinal relaxation rate (R_1) of the backbone ^{15}N nuclei of high-spin NP4 measured under various conditions, comparison of the transverse relaxation rate (R_2) of the backbone ^{15}N nuclei of high-spin NP4 measured under various conditions, comparison of $^{15}N\{^1H\}$ NOE parameters of high-spin NP4 measured under various conditions, ^{15}N relaxation data and calculated model-free order parameters (S^2) of the high-spin native N-terminal NP4 measured at pH 7.3 and 1.0 mM, obtained at 600 MHz, ^{15}N relaxation data and calculated model-free order parameters (S^2) of the native N-terminal NP4 measured at pH 6.5, 600 MHz, and 0.8 and 0.2 mM, comparison of generalized order parameters (S^2) of high-spin NP4(sym) obtained using relaxation parameters measured under various conditions, plot of the change in k_{ex} at pH 6.5 (k_{ex} at 0.2 mM − k_{ex} at 0.8 mM), with estimated error bars, pictures comparing the H-bonding between β-strands A and H of NP4 and NP2, plots of CPMG fits at pH 6.5 (0.8 mM) and pH 7.3 (1.0 mM) for each residue, and plots of CPMG fits at pH 6.5 and 0.2 and 0.8 mM for each residue. In addition to these figures, there are 15 tables of experimental data: high-spin NP4(sym) chemical shifts, summary of the *TALOS-N* output from analysis of high-spin NP4(sym) backbone chemical shifts, ^{15}N longitudinal relaxa-

DOI: 10.1021/bi501305a
Biochemistry 2015, 54, 221−239

tion rates (R_1) measured for high-spin NP4(sym) at two pH values, ^{15}N transverse relaxation rates (R_2) measured for high-spin NP4(sym) at two pH values, $^{15}N\{^1H\}$ NOE data measured for high-spin NP4(sym) at two pH values, backbone dynamic parameters from model-free calculations of ^{15}N spin relaxation data for high-spin NP4(sym) at pH 7.3, backbone dynamics parameters for model-free calculations of ^{15}N spin relaxation data for NP4(sym) at pH 6.5, summary of model selection in the model-free calculations using relaxation parameters measured at two pH values, NP4(sym) CPMG results at pH 7.3 (1.0 mM), including N−Fe distances from PDB entry 3C78, CPMG results at pH 6.5, a list of changes in NP4(sym) CPMG results between pH 7.3 and 6.5, a list of high-spin NP2 R_1, R_2, and NOE data recorded at pH 7.3, CPMG results for high-spin NP2 at pH 7.3, the last two listed by peak number, and a sample FAST-Modelfree configuration file used in the NP4 calculations. An Appendix of complete sequence-specific assignment tables for $[^{13}C,^{15}N]$NP4 obtained at pH 7.3, assignments from the $^1H\{^{15}N\}$ HSQC experiment (Table A1), $^{13}C_\alpha$ assignments from the HNCA experiment (Table A2), ^{13}CO assignments from the HNCO and HN(CA)CO experiments (Table A3), and $^{13}C_\alpha$ and $^{13}C_\beta$ assignments from the HNCACB and CBCA(CO)NH experiments (Table A4). This material is available free of charge via the Internet at http://pubs.acs.org.

AUTHOR INFORMATION

Corresponding Authors

*E-mail: rberry@umassd.edu. Telephone: (520) 399-8804.
*E-mail: dhanas.muthu@gmail.com. Telephone: (520) 360-3385.
*E-mail: awalker@email.arizona.edu. Telephone: (520) 621-8645.

Present Addresses

†R.B.: Department of Chemistry & Biochemistry, University of Massachusetts—Dartmouth, SENG-311A, 285 Old Westport Rd., North Dartmouth, MA 02747.
‡D.M.: 13606 Legacy Circle B, Herndon, VA 20171.

Author Contributions

This work was supported by National Institutes of Health Grant HL054826. This study also made use of the National Magnetic Resonance Facility at Madison (NMRFAM), which is supported by National Institutes of Health Grants P41RR02301 (Biomedical Research Technology Program, National Center for Research Resources) and P41GM66326 (National Institute of General Medical Sciences). Equipment in the facility was purchased with funds from the University of Wisconsin, the National Institutes of Health (P41GM66326, P41RR02301, RR02781, and RR08438), the National Science Foundation (DMB-8415048, OIA-9977486, and BIR-9214394), and the U.S. Department of Agriculture.

Notes

The authors declare no competing financial interest.

ACKNOWLEDGMENTS

We acknowledge the help of and consultation with Dr. Marco Tonelli (NMRFAM) in running the NMR experiments, Erin Berry for assigning part of the $^1H\{^{15}N\}$ HSQC map of NP4 at pH 7.3, and Dr. Andrei Astashkin for help with the figures.

ADDITIONAL NOTES

[a]I. Filippov, R. E. Berry, and F. A. Walker, Solution Structure and H/D Exchange of Apo-Nitrophorin 2 from *Rhodnius prolixus* Determined by Multidimensional NMR Spectroscopy. Manuscript to be submitted in 2015.
[b]See ref 18 and Table S1 of the Supporting Information.

REFERENCES

(1) Ribeiro, J. M. C., Hazzard, J. M. H., Nussenzveig, R. H., Champagne, D. E., and Walker, F. A. (1993) Reversible Binding of Nitric Oxide by a Salivary Heme Protein from a Bloodsucking Insect. *Science 260*, 539−541.
(2) Champagne, D. E., Nussenzveig, R., and Ribeiro, J. M. C. (1995) Purification, Partial Characterization, and Cloning of Nitric Oxide-carrying Heme proteins (Nitrophorins) from Salivary Glands of the Blood-sucking Insect *Rhodnius prolixus*. *J. Biol. Chem. 270*, 8691−8695.
(3) Valenzuela, J. G., Walker, F. A., and Ribeiro, J. M. C. (1995) A Salivary Nitrophorin (NO-Carrying Heme Protein) in the Bedbug, *Cimex lectularius*. *J. Exp. Biol. 198*, 1519−1526.
(4) Walker, F. A. (2005) Nitric Oxide Interaction with Insect Nitrophorins, and Thoughts on the Electron Configuration of the $\{FeNO\}^6$ Complex. *J. Inorg. Biochem. 99*, 216−236.
(5) Weichsel, A., Andersen, J. F., Champagne, D. E., Walker, F. A., and Montfort, W. R. (1998) Crystal Structures of a Nitric Oxide Transport Protein from a Blood-Sucking Insect. *Nat. Struct. Biol. 5*, 304−309.
(6) Ding, X. D., Weichsel, A., Balfour, C., Shokhireva, T. K., Pierik, A., Averill, B. A., Montfort, W. R., and Walker, F. A. (1999) Nitric Oxide Binding to the Ferri- and Ferroheme States of Nitrophorin 1, a Reversible NO-Binding Heme Protein from the Saliva of a Blood-Sucking Insect, *Rhodnius prolixus*. *J. Am. Chem. Soc. 121*, 128−138.
(7) Berry, R. E., Ding, X. D., Shokhireva, T. K., Weichsel, A., Montfort, W. R., and Walker, F. A. (2004) Axial Ligand Complexes of the *Rhodnius* Nitrophorins: Electrochemistry, Binding Constants, and Structures of the 4-Iodopyrazole and Imidazole Complexes of NP4. *JBIC, J. Biol. Inorg. Chem. 9*, 135−144.
(8) Andersen, J. F., and Montfort, W. R. (2000) The Crystal Structure of Nitrophorin 2, A Trifunctional Antihemostatic Protein from the Saliva of *Rhodnius prolixus*. *J. Biol. Chem. 275*, 30496−30503.
(9) Weichsel, A., Berry, R. E., Zhang, H., Walker, F. A., and Montfort, W. R. Crystal Structures, Conformational Change and Heme Deformation in Complexes of Nitrophorin 2, a Nitric Oxide Transport Protein from *Rhodnius prolixus*. PDB entries 1PEE, 1PM1, 1T68, 2A3F, 2ACP, 2AH7, 2AL0, 2ALL, 2AMM, 2ASN, 2EU7, 2HYS, and 2GTF.
(10) Andersen, J. F., Weichsel, A., Balfour, C., Champagne, D. E., and Montfort, W. R. (1998) The Crystal Structure of Nitrophorin 4 at 1.5 Å Resolution: Transport of Nitric Oxide by a Lipocalin-Based Heme Protein. *Structure 6*, 1315−1327.
(11) Weichsel, A., Andersen, J. F., Roberts, S. A., and Montfort, W. R. (2000) Nitric Oxide Binding to Nitrophorin 4 Induces Complete Distal Pocket Burial. *Nat. Struct. Biol. 7*, 551−554.
(12) Roberts, S. A., Weichsel, A., Qiu, Y., Shelnutt, J. A., Walker, F. A., and Montfort, W. R. (2001) Ligand-Induced Heme Ruffling and Bent NO Geometry in Ultra-High-Resolution Structures of Nitrophorin 4. *Biochemistry 40*, 11327−11337.
(13) Maes, E. M., Weichsel, A., Andersen, J. F., Shepley, D., and Montfort, W. R. (2004) Role of Binding Site Loops in Controlling Nitric Oxide Release: Structure and Kinetics of Mutant Forms of Nitrophorin 4. *Biochemistry 43*, 6679−6690.
(14) Maes, E. M., Roberts, S. A., Weichsel, A., and Montfort, W. R. (2005) Ultrahigh Resolution Structures of Nitrophorin 4: Heme Distortion in Ferrous CO and NO Complexes. *Biochemistry 44*, 12690−12699.
(15) Kondrashov, D. A., Roberts, S. A., Weichsel, A., and Montfort, W. R. (2004) Protein Functional Cycle Viewed at Atomic Resolution: Conformational Change and Mobility in Nitrophorin 4 as a Function of pH and NO Binding. *Biochemistry 43*, 13637−13647.

DOI: 10.1021/bi501305a
Biochemistry 2015, 54, 221−239

(16) Yuda, M., Hirai, M., Miura, K., Matsumura, H., Ando, K., and Chinzei, Y. (1996) cDNA Cloning, Expression and Characterization of Nitric-Oxide Synthase from the Salivary Glands of the Blood-Sucking Insect *Rhodnius prolixus*. *Eur. J. Biochem. 242*, 807−812.
(17) Poulos, T. L. (2006) Soluble guanylate cyclase. *Curr. Opin. Struct. Biol. 16*, 736−743.
(18) Berry, R. E., Muthu, D., Garrett, S. A., Shokhireva, T. K., Zhang, H., and Walker, F. A. (2012) Native N-Terminus Nitrophorin 2 from the Kissing Bug: Similarities to and Differences from NP2(D1A). *Chem. Biodiversity 9*, 1739−1755.
(19) Andersen, J. F., Ding, X. D., Balfour, C., Champagne, D. E., Walker, F. A., and Montfort, W. R. (2000) Kinetics and Equilibria in Ligand Binding by Nitrophorins 1−4: Evidence for Stabilization of a NO-Ferriheme Complex through a Ligand-Induced Conformational Trap. *Biochemistry 39*, 10118−10131.
(20) Nienhaus, K., Maes, E. M., Weichsel, A., Montfort, W. R., and Nienhaus, G. U. (2004) Structural Dynamics Controls Nitric Oxide Affinity in Nitrophorin 4. *J. Biol. Chem. 279*, 39401−39407.
(21) Kubo, M., Gruia, F., Benabbas, A., Barabanschikov, A., Montfort, W. R., Maes, E. M., and Champion, P. M. (2008) Low-Frequency Mode Activity of Heme: Femtosecond Coherence Spectroscopy of Iron Porphine Halides and Nitrophorin. *J. Am. Chem. Soc. 130*, 9800−9811.
(22) Benabbas, A., Ye, X., Kubo, M., Zhang, Z., Maes, E. M., Montfort, W. R., and Champion, P. M. (2010) Ultrafast Dynamics of Diatomic Ligand Binding to Nitrophorin 4. *J. Am. Chem. Soc. 132*, 2811−2820.
(23) Cheng, M., Brookes, J. P., Montfort, W. R., and Khalil, M. (2013) pH-Dependent Picosecond Structural Dynamics in the Distal Pocket of Nitrophorin 4 Investigated by 2D IR Spectroscopy. *J. Phys. Chem. B 117*, 15804−15811.
(24) Abbruzzetti, S., He, C., Ogata, H., Bruno, S., Viappiani, C., and Knipp, M. (2012) Heterogeneous Kinetics of the Carbon Monoxide Association and Dissociation Reaction to Nitrophorin 4 and 7 Coincide with Structural Heterogeneity of the Gate-Loop. *J. Am. Chem. Soc. 134*, 9986−9998.
(25) Muthu, D., Berry, R. E., Zhang, H., and Walker, F. A. (2013) NMR Studies of the Dynamics of Nitrophorin 2 Bound to Nitric Oxide. *Biochemistry 52*, 7910−7925.
(26) Lipari, G., and Szabo, A. (1982) Model-free Approach to the Interpretation of Nuclear Magnetic Resonance Relaxation in Macromolecules. 1. Theory and Range of Validity. *J. Am. Chem. Soc. 104*, 4546−4559.
(27) Lipari, G., and Szabo, A. (1982) Model-free Approach to the Interpretation of Nuclear Magnetic Resonance Relaxation in Macromolecules. 2. Analysis of Experimental Results. *J. Am. Chem. Soc. 104*, 4559−4570.
(28) Clore, G. M., Szabo, A., Bax, A., Kay, L. E., Driscoll, P. C., and Gronenborn, A. M. (1990) Deviations from the Simple Two Parameter Model Free Approach to the Interpretation of ^{15}N Nuclear Magnetic Relaxation of Proteins. *J. Am. Chem. Soc. 112*, 4989−4991.
(29) Clore, G. M., Driscoll, P. C., Wingfield, P. T., and Gronenborn, A. M. (1990) Analysis of Backbone Dynamics of Interlukin 1β Using Two-dimensional Inverse Detected Heteronuclear ^{15}N-^{1}H NMR Spectroscopy. *Biochemistry 29*, 7387−7401.
(30) Farrow, N. A., Muhandham, J. R., Singer, A. J., Pascal, S. M., Kay, C. M., Gish, G., Shoelson, S. E., Pawson, T., Forman-Kay, J. D., and Kay, L. E. (1994) Backbone Dynamics of a Free and a Phosphopeptide-Complexed Src Homology 2 Domain Studied by ^{15}N NMR Relaxation. *Biochemistry 33*, 5984−6003.
(31) Mandel, A. M., Akke, M., and Palmer, A. G. (1995) Backbone Dynamics of *Escherichia coli* Ribonuclease HI: Correlations with Structure and Function in an Active Enzyme. *J. Mol. Biol. 246*, 144−163.
(32) Cole, R., and Loria, J. P. (2003) FAST-Modelfree: A Program for Rapid Automated Analysis of Solution NMR Spin-Relaxation Data. *J. Biomol. NMR 26*, 203−213.
(33) Mulder, F. A. A., Hon, B., D. Muhandiram, R., Dahlquist, F. W., and Kay, L. E. (2000) Flexibility and Ligand Exchange in a Buried Cavity Mutant of T4 Lysozyme Studied by Multinuclear NMR. *Biochemistry 39*, 12614−12622.
(34) Tollinger, M., Skrynnikov, N. R., Mulder, F. A. A., Forman-Kay, J. D., and Kay, L. E. (2001) Slow Dynamics in Folded and Unfolded States of an SH3 Domain. *J. Am. Chem. Soc. 123*, 11341−11352.
(35) Korzhnev, D. M., and Kay, L. E. (2008) Probing Invisible, Low-Populated States of Protein Molecules by Relaxation Dispersion NMR Spectroscopy: An Application to Protein Folding. *Acc. Chem. Res. 41*, 442−451.
(36) Palmer, A. G. (2004) NMR Characterization of the Dynamics of Biomacromolecules. *Chem. Rev. 104*, 3623−3640.
(37) Eisenmesser, E. Z., Millet, O., Labeikovsky, W., Korzhnev, D. M., Wolf-Watz, M., Bosco, D. A., Skalickey, J. J., Kay, L. E., and Kern, D. (2005) Intrinsic Dynamics of an Enzyme Underlies Catalysis. *Nature 438*, 117−121.
(38) Boehr, D. D., McElheny, D., Dyson, H. J., and Wright, P. E. (2006) The Dynamic Energy Landscape of Dihydrofolate Reductase Catalysis. *Science 313*, 1638−1642.
(39) Korzhnev, D. M., Religa, T. L., Banachewicz, W., Fersht, A. R., and Kay, L. E. (2010) A Transient and Low-Populated Protein-Folding Intermediate at Atomic Resolution. *Science 329*, 1312−1316.
(40) Bouvignies, G., Hansen, D. F., Vallurupalli, P., and Kay, L. E. (2011) Divided-Evolution-Based Pulse Scheme for Quantifying Exchange Processes in Proteins: Powerful Complement to Relaxation Dispersion Experiments. *J. Am. Chem. Soc. 133*, 1935−1945.
(41) Hodsdon, M., and Cistola, D. P. (1997) Ligand Binding Alters the Backbone Mobility of Intestinal Fatty Acid-Binding Protein as Monitored by ^{15}N NMR Relaxation and ^{1}H Exchange. *Biochemistry 36*, 2278−2290.
(42) Qin, B. Y., Creamer, L. K., Baker, E. N., and Jameson, G. B. (1998) 12-Bromododecanoic Acid Binds inside the Calyx of Bovine β-Lactoglobulin. *FEBS Lett. 438*, 272−278.
(43) Narayn, M., and Berliner, L. J. (1997) Fatty Acids and Retinoids Bind Independently and Simultaneously to β-Lactoglobulin. *Biochemistry 36*, 1905−1911.
(44) Dufour, E., Marden, M. C., and Haertlé, T. (1990) β-Lactoglobulin Binds Retinol and Protoporphyrin IX at Two Different Binding Sites. *FEBS Lett. 277*, 223−226.
(45) Brownlow, S., Morais Cabral, J. H., Cooper, R., Flower, D. R., Yewdall, S. J., Polikarpov, I., North, A. C. T., and Sawyer, L. (1997) Bovine β-Lactoglobulin at 1.8 Å Resolution: Still an Enigmatic Lipocalin. *Structure 5*, 481−495.
(46) Kuwata, K., Hoshino, M., Forge, V., Era, S., Batt, C. A., and Goto, Y. (1999) Solution Structure and Dynamics of Bovine β-Lactoglobulin. *Protein Sci. 8*, 2541−2545.
(47) Uhrinova, S., Smith, M. H., Jameson, G. B., Uhrin, D., Sawyer, L., and Barlow, P. N. (2000) Structural Changes Accompanying pH-Induced Dissociation of the β-Lactoglobulin Dimer. *Biochemistry 39*, 3565−3574.
(48) Ragona, L., Catalano, M., Luppi, M., Cicero, D., Elisea, T., Foote, J., Fogolari, F., Zetta, L., and Molinari, H. (2006) NMR Dynamic Studies Suggest that Allosteric Activation Regulates Ligand Binding in Chicken Liver Bile Acid-binding Protein. *J. Biol. Chem. 281*, 9697−9709.
(49) Mills, J. L., Liu, G., Skerra, A., and Szyperski, T. (2009) NMR Structure and Dynamics of the Engineered Fluorescein-Binding Lipocalin, FluA Reveal Rigidification of β-Barrel and Variable Loops upon Enthalpy-Driven Ligand Binding. *Biochemistry 48*, 7411−7419.
(50) Horváth, G., Király, P., Tárkányi, G., and Toke, O. (2012) Internal Motions and Exchange Processes in Human Ileal Bile Acid Binding Protein As Studied by Backbone ^{15}N Nuclear Magnetic Resonance Spectroscopy. *Biochemistry 51*, 1848−1861.
(51) Berry, R. E., Muthu, D., Shokhireva, T. K., Garrett, S. A., Goren, A. M., Zhang, H., and Walker, F. A. (2014) NMR Investigations of Nitrophorin 2 Belt Side Chain Effects on Heme Orientation and Seating of Native N-Terminus NP2 and NP2(D1A). *JBIC, J. Biol. Inorg. Chem. 2014* (19), 577−593.

DOI: 10.1021/bi501305a
Biochemistry 2015, 54, 221−239

(52) La Mar, G. N., and de Ropp, J. S. (1993) NMR Methodology for Paramagnetic Proteins. In *Biological Magnetic Resonance* (Berliner, L. J., and Reuben, J., Eds.) Vol. *12*, pp 1−78, Plenum Press, New York.
(53) Banci, L., Bertini, I., Cavazza, C., Felli, I. C., and Koulougliotis, D. (1998) Probing the Backbone Dynamics of Oxidized and Reduced Rat Microsomal Cytochrome b_5 via ^{15}N Rotating Frame NMR Relaxation Measurements: Biological Implications. *Biochemistry 37*, 12320−12330.
(54) Banci, L., Felli, I. C., and Koulougliotis, D. (1998) Identification of Slow Motions in the Reduced Recombinant High-Potential Iron Sulfur Protein I (HiPiP) from *Ectothiorhodospira halophila* via ^{15}N Rotating Frame NMR Relaxation Experiments. *J. Biol. NMR 12*, 307−318.
(55) Abriata, L. A., Zaballa, M.-E., Berry, R. E., Yang, F., Zhang, H., Walker, F. A., and Vila, A. J. (2013) Electron Spin Density on the Axial His Ligand of High-Spin and Low-Spin Nitrophorin 2 Probed by Heteronuclear NMR Spectroscopy. *Inorg. Chem. 52*, 1285−1295.
(56) Andersen, J. F., Champagne, D. E., Weichsel, A., Ribeiro, J. M. C., Balfour, C. A., Dress, V., and Montfort, W. R. (1997) Nitric Oxide Binding and Crystallization of Recombinant Nitrophorin 1, a Nitric Oxide Transport Protein from the Blood-Sucking Bug *Rhodnius prolixus*. *Biochemistry 36*, 4423−4428.
(57) Shokhireva, T. K., Shokhirev, N. V., Berry, R. E., Zhang, H., and Walker, F. A. (2008) Assignment of Ferriheme Resonances for High- and Low-Spin Forms of the Symmetrical Hemin-Reconstituted Nitrophorins 1−4 by ^{1}H and ^{13}C NMR Spectroscopy: The Dynamics of Heme Ruffling Deformations. *JBIC, J. Biol. Inorg. Chem. 13*, 941−959.
(58) Berry, R. E., Shokhireva, T. K., Filippov, I., Shokhirev, M. N., Zhang, H., and Walker, F. A. (2007) Effect of the N-Terminus on Heme Cavity Structure, Ligand Equilibrium and Rate Constants, and Reduction Potentials of Nitrophorin 2 from *Rhodnius prolixus*. *Biochemistry 46*, 6830−6843.
(59) Bahrami, A., Assadi, A. H., Markley, J. L., and Eghbalnia, H. R. (2009) Probabilistic Interaction Network of Evidence Algorithm and Its Application to Complete Labeling of Peak Lists from Protein NMR Spectroscopy. *PLoS Comput. Biol. 5* (3), e1000307.
(60) Lee, W., Westler, W. M., Bahrami, A., Eghbalnia, H. R., and Markley, J. L. (2009) PINE-SPARKY: Graphical Interface for Evaluating Automated Probabilistic Peak Assignments in Protein NMR Spectroscopy. *Bioinformatics 25*, 2085−2087.
(61) Markley, J. L., Bax, A., Arata, Y., Hilbers, C. W., Kaptein, R., Sykes, B. D., Wright, P. E., and Wüthrich, K. (1998) Recommendations for the Presentation of NMR Structures of Proteins and Nucleic Acids. *Eur. J. Biochem. 256*, 1−15.
(62) Cornilescu, G., Delaglio, F., and Bax, A. (1999) Protein Backbone Angle Restraints from Searching a Database for Chemical Shift and Sequence Homology. *J. Biomol. NMR 13*, 289−302.
(63) Shen, Y., Delaglio, F., Cornilescu, G., and Bax, A. (2009) TALOS+: A Hybrid Method for Predicting Protein Backbone Torsion Angles from NMR Chemical Shifts. *J. Biomol. NMR 44*, 213−223.
(64) Shen, Y., and Bax, A. (2013) Protein Backbone and Sidechain Torsion Angles Predicted from NMR Chemical Shifts Using Artificial Neural Networks. *J. Biomol. NMR 56*, 227−241.
(65) Berjanskii, M. V., and Wishart, D. S. (2005) A Simple Method To Predict Protein Flexibility Using Secondary Chemical Shifts. *J. Am. Chem. Soc. 127*, 14970−14971.
(66) Delaglio, F., Grzesiek, S., Vuister, G. W., Zhu, G., Pfeifer, J., and Bax, A. (1995) NMRPipe: A Multidimensional Spectral Processing System Based on UNIX Pipes. *J. Biomol. NMR 6*, 277−293.
(67) Delaglio, F. (2006−2012) *NMRPipe: A Comprehensive Software System for Multidimensional NMR Applications* (http://www.nmrscience.com/nmrpipe.html).
(68) Goddard, T. D., and Kneller, D. G. (2008) *SPARKY 3*, version 3.115, University of California, San Francisco (http://www.cgl.ucsf.edu/home/sparky/).
(69) Bieri, M., d'Auvergne, E. J., and Gooley, P. R. (2011) *RelaxGUI*: A new software for fast and simple NMR relaxation data analysis and calculation of ps-ns and μs motion of proteins. *J. Biomol. NMR 50*, 147−155.
(70) Brüschweiler, R., Liao, X., and Wright, P. E. (1995) Long-range motional restrictions in a multi-domain zinc-finger protein from anisotropic tumbling. *Science 268*, 886−889.
(71) Lee, A. L., Urbauer, J. L., and Wand, A. J. (1997) Improved labeling strategy for ^{13}C relaxation measurements of methyl groups in proteins. *J. Biomol. NMR 9*, 437−440.
(72) Pettersen, E. F., Goddard, T. D., Huang, C. C., Couch, G. S., Greenblatt, D. M., Meng, E. C., and Ferrin, T. E. (2004) UCSF Chimera: A visualization system for exploratory research and analysis. *J. Comput. Chem. 25*, 1605−1612.
(73) Bieri, M., and Gooley, P. R. (2011) Automated NMR Relaxation Dispersion Data Analysis Using NESSY. *BMC Bioinf. 12*, 421.
(74) Morin, S. B. (2011) A Practical Guide to Protein Dynamics from ^{15}N Spin Relaxation in Solution. *Prog. NMR Spectrosc. 59*, 245−262.
(75) Kleckner, I. R., and Foster, M. P. (2011) An Introduction to NMR-based Approaches for Measuring Protein Dynamics. *Biochim. Biophys. Acta 1814*, 942−968.
(76) d'Auvergne, E. J., and Gooley, P. R. (2008) Optimisation of NMR dynamic models I. Minimisation algorithms and their performance within the model-free and Brownian rotational diffusion spaces. *J. Biomol. NMR 40* (2), 107−119.
(77) d'Auvergne, E. J., and Gooley, P. R. (2008) Optimisation of NMR dynamic models II. A new methodology for the dual optimization of the model-free parameters and the Brownian rotational diffusion tensor. *J. Biomol. NMR 40* (2), 121−133.
(78) http://www.nmr-relax.com/.
(79) Palmer, A. G., Rance, M., and Wright, P. E. (1991) Intramolecular motions of a zinc finger DNA-binding domain from Xfin characterized by proton-detected natural abundance ^{13}C heteronuclear NMR spectroscopy. *J. Am. Chem. Soc. 113*, 4371−4380.
(80) Kempf, J. G., and Loria, J. P. (2003) Protein Dynamics from Solution NMR: Theory and Applications. *Cell Biochem. Biophys. 37*, 187−211.
(81) Amoia, A. M., and Montfort, W. R. (2007) Apo-Nitrophorin 4 at Atomic Resolution. *Protein Sci. 16*, 2076−2081.
(82) The k_d values are taken from Table 3 of the companion paper (DOI: 10.1021/bi5013047).

DOI: 10.1021/bi501305a
Biochemistry 2015, 54, 221−239